# Ultimate Limits of Reinforced Concrete Hinges

Thomas Schlappal[a], Johannes Kalliauer[a], Markus Vill[b], Herbert A. Mang[a,c], Josef Eberhardsteiner[a], Bernhard L.A. Pichler[a,*]

[a] *TU Wien – Vienna University of Technology, Institute for Mechanics of Materials and Structures, Karlsplatz 13/202, AT-1040 Vienna, Austria*
[b] *Vill Ziviltechniker GmbH, Hermanngasse 18, AT-1070 Vienna, Austria*
[c] *Tongji University, College of Civil Engineering, Siping Road 1239, CN-200092 Shanghai, China*

---

**Abstract**

This work is a further development of its predecessor, the topic of which was verification of serviceability limit states of reinforced concrete hinges. Herein, the same conceptual approach is used to derive analytical formulae, supporting verification of ultimate limit states. These formulae limit tolerable relative rotations as a function of the compressive normal force transmitted across the neck. The mechanical model is based on the Bernoulli-Euler hypothesis and on linear-elastic and ideally-plastic stress-strain relationships for both concrete in compression and steel in tension. The usefulness of the derived formulae and the corresponding dimensionless design diagrams is assessed by means of experimental data from structural testing of reinforced concrete hinges, taken from the literature. This way, it is shown that the proposed mechanical model is suitable for describing ultimate limit states. Corresponding design recommendations are elaborated and exemplarily applied to verification of ultimate limit states of the reinforced concrete hinges of a recently built integral bridge. Since the reinforcement is explicitly accounted for, the tolerable relative rotations are larger than those according to existing guidelines. It is included that bending-induced tensile macrocracking beyond one half of the smallest cross-section of the neck is acceptable, because the tensile forces carried by the reinforcement ensure the required position stability of the hinges.

*Corresponding author
*Email address:* bernhard.pichler@tuwien.ac.at (Bernhard L.A. Pichler)

*Preprint submitted to Engineering Structures* *June 2, 2020*

This document is the accepted version of a work that was published in Engineering Structures. To access the final edited and published work see, https://doi.org/10.1016/j.engstruct.2020.110889.

*Keywords:* Ultimate limit states (ULS), integral bridges, design recommendations

## 1. Introduction

Concrete hinges are marginally reinforced necks in reinforced concrete structures, see Fig. 1. They are used, e.g., as supports in integral bridge construction. Because of the throat, threedimensional compressive stress states are activated in the region of the neck. The resulting confinement of the concrete increases both its strength and ductility. Current design standards, such as the Eurocode [1, 2, 3, 4], require the verification of serviceability and ultimate limit states prior to the construction of reinforced concrete structures. This provided the motivation for the companion paper [5] and the present contribution.

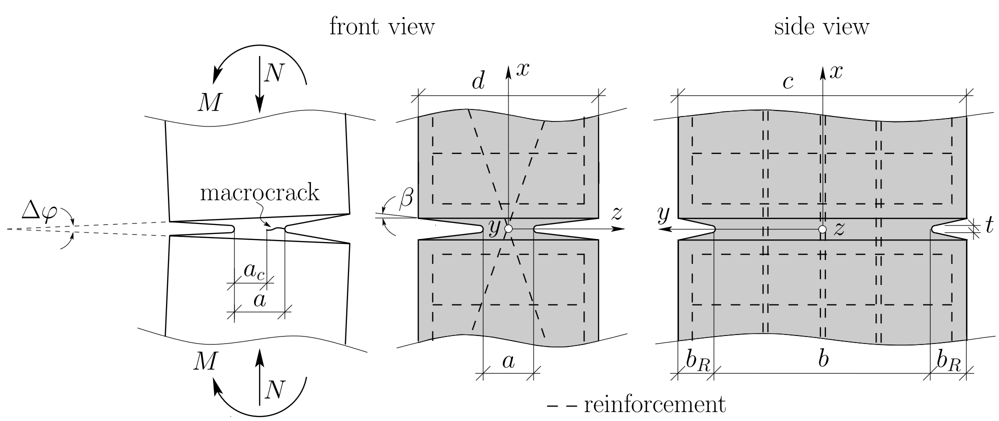


Figure 1: Geometric dimensioning of a concrete hinge with reinforcement crossing at the centerline of the neck; $a_c$ denotes the width of the compressed ligament [5]

Recommendations for the verification of serviceability limit states of reinforced concrete hinges were the focus of a previous paper [5]. The engineering mechanics approach of Leonhardt and Reimann [6] was extended in order to account explicitly for centrally crossing steel rebars. Linear-elastic material behavior was assumed for concrete in compression and for steel in tension. The tensile strength of concrete was set equal to zero. The steel rebars were accounted for only if subjected to tension. The Bernoulli-Euler hypothesis was used to derive analytical expressions for elastic limit states of reinforced concrete hinges. They are assumed to occur if the maximum compressive normal stress of concrete reaches the triaxial compressive strength and/or if the steel rebars start to yield. This approach allowed for assigning a maximum tolerable relative rotation to each value of the normal force transmitted across the neck. Results were illustrated in the form of dimensionless diagrams. Comparing model-predicted elastic limits with results from structural testing, it was shown that the modeling approach is useful for specification of serviceability limit states of reinforced concrete hinges. Finally, recommendations regarding verification of serviceability limit states were elaborated. They were used for the *a posteriori* verification of the reinforced concrete hinges of an integral bridge in Austria. Since the reinforcement was explicitly accounted for, the serviceability limits of relative rotations are *larger* than those according to the guidelines of Leonhardt and Reimann [6].

Recommendations for verification of ultimate limit states of reinforced concrete hinges are the focus of the present paper. The target is the derivation of analytical formulae, describing maximum tolerable relative rotations as a function of the normal force transmitted across the neck. To this end, linear-elastic and ideally-plastic material behavior is assumed for concrete in compression and for steel in tension. The triaxial compressive strength of concrete is estimated based on regulations regarding partially loaded areas [1]. The tensile strength of concrete is set equal to zero. The steel rebars are accounted for only if subjected to tension.

The Bernoulli-Euler hypothesis is used to derive analytical expressions for ultimate limit states of reinforced concrete hinges. These limits are assumed to occur if the maximum compressive normal strain of concrete and/or if the maximum tensile normal strain of the steel rebars reach the corresponding ultimate limit strain. The analysis involves consideration of six different operating conditions of reinforced concrete hinges. Notably, the ultimate limit strain of concrete subjected to triaxial compression is still not fully understood. This provides the motivation to perform sensitivity analyses with respect to different confinement levels. It is based on recommendations for the effective strength of concrete in the core of reinforced concrete columns [7].

The extended engineering mechanics model is used to derive analytical formulae as the basis for dimensionless diagrams. They illustrate the limits of the tolerable relative rotation as a function of the transmitted normal force. The formulae and, hence, the dimensionless diagrams can be specified for specific geometric and material properties of reinforced concrete hinges. The usefulness of the described approach is assessed with the help of experimental data taken from the open literature. Subsequently, recommendations for verification of ultimate limit states of reinforced concrete hinges are elaborated. They are applied to *a posteriori* verification of the reinforced concrete hinges of an integral bridge in Austria [8].

The present paper is structured as follows. Section 2 contains the theoretical description of ultimate limits of reinforced concrete hinges. Section 3 deals with an assessment of the derived formulae by means of experimental data taken from the open literature. Section 4 is devoted to recommendations for verification of ultimate limit states of reinforced concrete hinges and to their application to the aforementioned bridge. The paper ends with a discussion (Section 5), followed by conclusions (Section 6).

## 2. Theoretical investigation of ultimate limits of reinforced concrete hinges

Double-symmetric reinforced concrete hinges are geometrically described by means of Cartesian coordinates $x, y, z$, see Fig. 1. In this illustration, $a$ denotes the width and $b$ the depth of the neck, $b_R$ the depth of the front-side notches, $c$ the depth of the adjacent reinforced concrete parts, $d$ their width, $t$ the height of the throat of the neck, and $\beta$ the opening angle of the throat.

Analytical formulae, expressing the normal force $N$ as a function of both the change of length in the $x$-direction, $\Delta\ell$, and the relative rotation $\Delta\varphi$, are derived in the following. Thereby, $\Delta\ell > 0$ indicates an elongation and $\Delta\ell < 0$ a shortening of the neck, see Fig. 2. The neck is idealized as a cuboid with geometric dimensions $a$, $b$, and $a$, in the $x$, $y$, and $z$-direction, respectively, see Fig. 2.

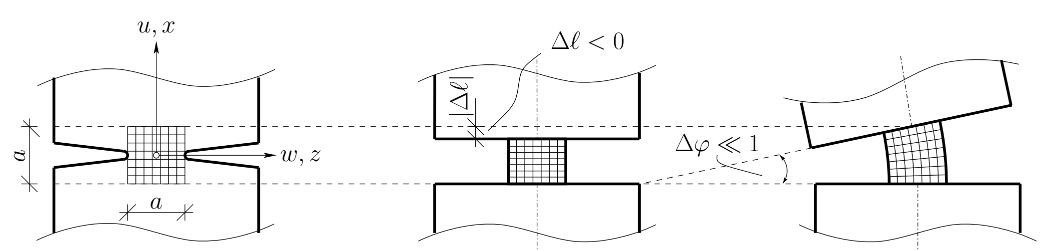


Figure 2: Idealized concrete hinge subjected to axial shortening $\Delta\ell < 0$ and to a relative rotation $\Delta\varphi$; the out-of-plane dimension $b$ of the neck is not shown [5]

### *2.1. Derivation of an expression for $N$ as a function of $\Delta\ell$ and $\Delta\varphi$*

The Bernoulli-Euler hypothesis is used. This leads to the following expression for the axial normal strain [5],

$$\varepsilon = \frac{\Delta\ell}{a} + \frac{\Delta\varphi}{a}\,z\,. \tag{1}$$

Eq. (1) underlines that the slope of $\varepsilon$ along the $z$-axis is proportional to $\Delta\varphi$ [5]:

$$\frac{\partial\varepsilon}{\partial z} = \frac{\Delta\varphi}{a}\,. \tag{2}$$

In order to calculate the axial normal stresses, linear-elastic, ideally-plastic material behavior is assumed for both concrete and steel. This is consistent with both the *fib* Model Code 2010 [7] and the Eurocode 2 [1].

It is assumed that concrete is unable to carry tension. Regarding compression, linear-elastic material behavior is assumed up to the elastic limit stress $|Ff_c|$. The symbol $F$ denotes the triaxial-to-uniaxial compressive strength ratio. It is estimated based on the Eurocode-recommendations for partially loaded areas [1, 5, 9, 10, 11] as:

$$F = \sqrt{F_a F_b}\,, \tag{3}$$

where $F_a$ and $F_b$ account for the lateral and the thickness contraction. They are defined as [5]

$$F_a = \min\left[\,3\ ;\ \frac{d}{a}\,\right], \tag{4}$$

and

$$F_b = \min\left[\,3\ ;\ \frac{c}{b}\,\right]. \tag{5}$$

Ideally plastic behavior refers to a stress plateau, extending from the elastic limit strain, $\varepsilon_{c,e}$, to the ultimate limit strain, $\varepsilon_{c,u}$:

$$\sigma_c = 0 \qquad \ldots\ldots\ldots\ldots\ldots\ldots \qquad \varepsilon_c \geq 0\,, \tag{6}$$

$$\sigma_c = -|Ff_c|\,\frac{\varepsilon}{\varepsilon_{c,e}} \qquad \ldots\ldots\ldots\ldots \qquad 0 \geq \varepsilon_c \geq \varepsilon_{c,e}\,, \tag{7}$$

$$\sigma_c = -|Ff_c| \qquad \ldots\ldots\ldots \qquad \varepsilon_{c,e} \geq \varepsilon_c \geq \varepsilon_{c,u}\,, \tag{8}$$

see Fig 3 (a). The values of $\varepsilon_{c,e}$ and $\varepsilon_{c,u}$ will be discussed in Subsection 2.9.

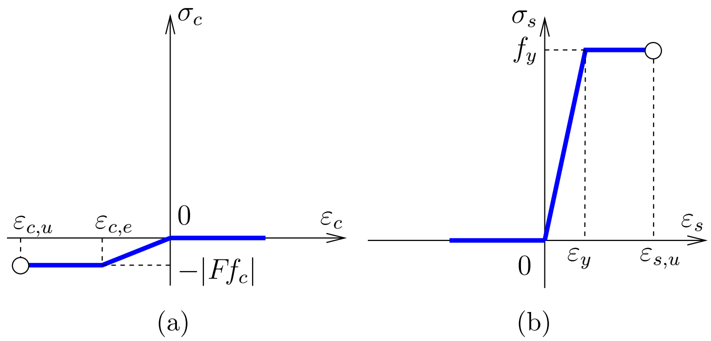


Figure 3: Linear-elastic and ideally-plastic material behavior of (a) concrete and (b) steel; $\sigma_c$, $\varepsilon$, and $|Ff_c|$, denote the normal stress, the normal strain, and the compressive strength of concrete, respectively; $\sigma_s$, $\varepsilon_s$, and $f_y$ stand for the normal stress, the normal strain, and the yield stress of steel, respectively

As for steel, the reinforcement is assumed to influence the structural behavior significantly only if subjected to tension. Thus, compressive stresses of steel are disregarded. In case of tension, steel is assumed to behave in a linear-elastic fashion up to the yield stress, $f_y$.[1] This is followed by a stress plateau, extending from the elastic limit strain, $\varepsilon_y$, to the ultimate limit strain of steel, $\varepsilon_{s,u}$:

$$\sigma_s = f_y \qquad \ldots\ldots\ldots \qquad \varepsilon_y \leq \varepsilon_s \leq \varepsilon_{s,u}\,, \tag{9}$$

$$\sigma_s = f_y\,\frac{\varepsilon_s}{\varepsilon_y} \qquad \ldots\ldots\ldots\ldots \qquad 0 \leq \varepsilon_s \leq \varepsilon_y\,, \tag{10}$$

$$\sigma_s = 0 \qquad \ldots\ldots\ldots\ldots\ldots\ldots \qquad \varepsilon_s \leq 0\,, \tag{11}$$

see Fig 3 (b). The values of $\varepsilon_y$ and $\varepsilon_{s,u}$ will be discussed in Subsection 2.9.

The normal force, which is transmitted across the neck, is equal to the integral of the axial normal stresses over the cross-sectional area $A$ of the neck [5]:

$$N = \int\limits_A \sigma \;\mathrm{d}A\,, \tag{12}$$

where $\mathrm{d}A = b\,\mathrm{d}z$. The width of the compressed ligament of concrete is

[1] Although conceptually desirable, no clear distinction between the proportionality limit and the elastic limit is made.

denoted as $a_c$, see Fig. 1. It is subdivided into two parts. Concrete behaves in an ideally-plastic fashion in the interval from $z=-a/2$ to $z=-a/2+a_p$, see also Fig. 4. Thus, $a_p$ denotes the width of the plastic ligament of concrete. Concrete behaves in a linear-elastic fashion in the interval from $z=-a/2+a_p$ to $z=-a/2+a_c$. Thus, Eq. (12) can be re-formulated as:

$$N = \int\limits_{-a/2}^{-a/2+a_p} -|Ff_c|\, b \; \mathrm{d}z + \int\limits_{-a/2+a_p}^{-a/2+a_c} \sigma_c\, b \; \mathrm{d}z + \sigma_s\, A_s\, \chi\,. \tag{13}$$

The third term on the right-hand-side of Eq. (13) refers to the reinforcement, with $A_s$ denoting the cross-sectional area of the rebars running across the neck. The factor $\chi$ is equal to 1 in case of tensile loading and equal to 0 otherwise:

$$\chi = \begin{cases} 1 & \ldots \quad \Delta\ell > 0\,, \\ 0 & \ldots \quad \Delta\ell \leq 0\,. \end{cases} \tag{14}$$

The sought expression for $N$ as a function of $\Delta\ell$ and $\Delta\varphi$ is obtained from inserting Eqs. (6)-(11) into Eq. (13), and specializing the resulting expressions for Eq. (1):

$$\begin{aligned} N \;\; = \;\; & -|Ff_c|\, b \left\{ a_p + \frac{1}{\varepsilon_{c,e}} \left[ \frac{\Delta\ell}{a}(a_c - a_p) + \frac{\Delta\varphi}{2} \left( \frac{a_c^2}{a} - a_c - \frac{a_p^2}{a} + a_p \right) \right] \right\} \\ & + \sigma_s\, \rho a b\, \chi\,, \end{aligned} \tag{15}$$

where $\rho$ denotes the reinforcement ratio [5]:

$$\rho = \frac{A_s}{ab}\,. \tag{16}$$

In Eq. (16), $ab$ denotes the cross-sectional area of the neck, see Fig. 1.

In order to transform $N$ into a dimensionless quantity, the degree of utilization $\nu$ is introduced [5]. It is equal to $N$ divided by the maximum compressive normal force that can be transmitted across the neck:

$$\nu = \frac{N}{-|Ff_c|\, ab} \leq 1\,. \tag{17}$$

The denominator in Eq. (17) refers to the maximum compressive normal force according Eq. (15). It is obtained in case of pure compression of the neck, where $\Delta\varphi = 0$, $a_c = a_p = a$, and $\chi = 0$.

### 2.2. *Ultimate limit states of reinforced concrete hinges for different operating conditions*

In the following, a maximum tolerable relative rotation $\Delta\varphi_\ell$ is assigned to every bearable degree of utilization of the normal force, $\nu$. Thereby, $\Delta\varphi_\ell$ corresponds to an ultimate limit state (ULS) of a reinforced concrete hinge. It is reached if the maximum compressive strain of the concrete is equal to the ultimate limit strain $\varepsilon_{c,u}$ and/or if the maximum tensile strain of the steel rebars is equal to the ultimate limit strain $\varepsilon_{s,u}$. Notably, the used model is based on linear strain distributions across the width of the neck, see Eq. (1). Seven specific strain distributions represent bounding scenarios for six operating conditions of reinforced concrete hinges, see Fig. 4. At operating conditions I to IV which are bounded by the scenarios (a) and (e), the ultimate limit strain of concrete is always reached at the left edge of the neck. At operating conditions V and VI which are bounded by the scenarios (e) and (g), the ultimate limit strain of steel is always reached. The corresponding state variables $\Delta\ell_\ell$, $\Delta\varphi_\ell$, $a_c$, $a_p$, $\chi$, $\sigma_s$, and $\nu$ are listed in Table 1.

Table 1: State variables associated with the ultimate limit states of reinforced concrete hinges illustrated in Fig. 4

| ULS | $\Delta\ell_\ell$ | $\Delta\varphi_\ell$ | $a_c$ | $a_p$ | $\chi$ | $\sigma_s$ | $\nu$ |
|---|---|---|---|---|---|---|---|
| (a) | $a\,\dfrac{(\varepsilon_{c,e}+\varepsilon_{c,u})}{2}$ | $(\varepsilon_{c,e}-\varepsilon_{c,u})$ | $a$ | $a$ | 0 | $\dfrac{f_y}{\varepsilon_y}\,\dfrac{\Delta\ell_\ell}{a}$ | 1 |
| (b) | $a\,\dfrac{\varepsilon_{c,u}}{2}$ | $-\varepsilon_{c,u}$ | $a$ | Eq. (22) | 0 | $\dfrac{f_y}{\varepsilon_y}\,\dfrac{\Delta\ell_\ell}{a}$ | $1-\dfrac{\varepsilon_{c,e}}{2\,\varepsilon_{c,u}}$ |
| (c) | 0 | $-2\,\varepsilon_{c,u}$ | $\dfrac{a}{2}$ | Eq. (22) | 0 | 0 | $\dfrac{1}{2}\left(1-\dfrac{\varepsilon_{c,e}}{2\,\varepsilon_{c,u}}\right)$ |
| (d) | $a\,\varepsilon_y$ | $2(\varepsilon_y-\varepsilon_{c,u})$ | Eq. (28) | Eq. (22) | 1 | $f_y$ | $\dfrac{\frac{1}{2}\varepsilon_{c,e}-\varepsilon_{c,u}}{2(\varepsilon_y-\varepsilon_{c,u})}-\dfrac{\rho\,f_y}{\lvert Ff_c\rvert}$ |
| (e) | $a\,\varepsilon_{s,u}$ | $2(\varepsilon_{s,u}-\varepsilon_{c,u})$ | Eq. (28) | Eq. (22) | 1 | $f_y$ | $\dfrac{\frac{1}{2}\varepsilon_{c,e}-\varepsilon_{c,u}}{2(\varepsilon_{s,u}-\varepsilon_{c,u})}-\dfrac{\rho\,f_y}{\lvert Ff_c\rvert}$ |
| (f) | $a\,\varepsilon_{s,u}$ | $2(\varepsilon_{s,u}-\varepsilon_{c,e})$ | Eq. (28) | 0 | 1 | $f_y$ | $\dfrac{-\varepsilon_{c,e}}{4(\varepsilon_{s,u}-\varepsilon_{c,e})}-\dfrac{\rho\,f_y}{\lvert Ff_c\rvert}$ |
| (g) | $a\,\varepsilon_{s,u}$ | $2\,\varepsilon_{s,u}$ | 0 | 0 | 1 | $f_y$ | $-\dfrac{\rho\,f_y}{\lvert Ff_c\rvert}$ |

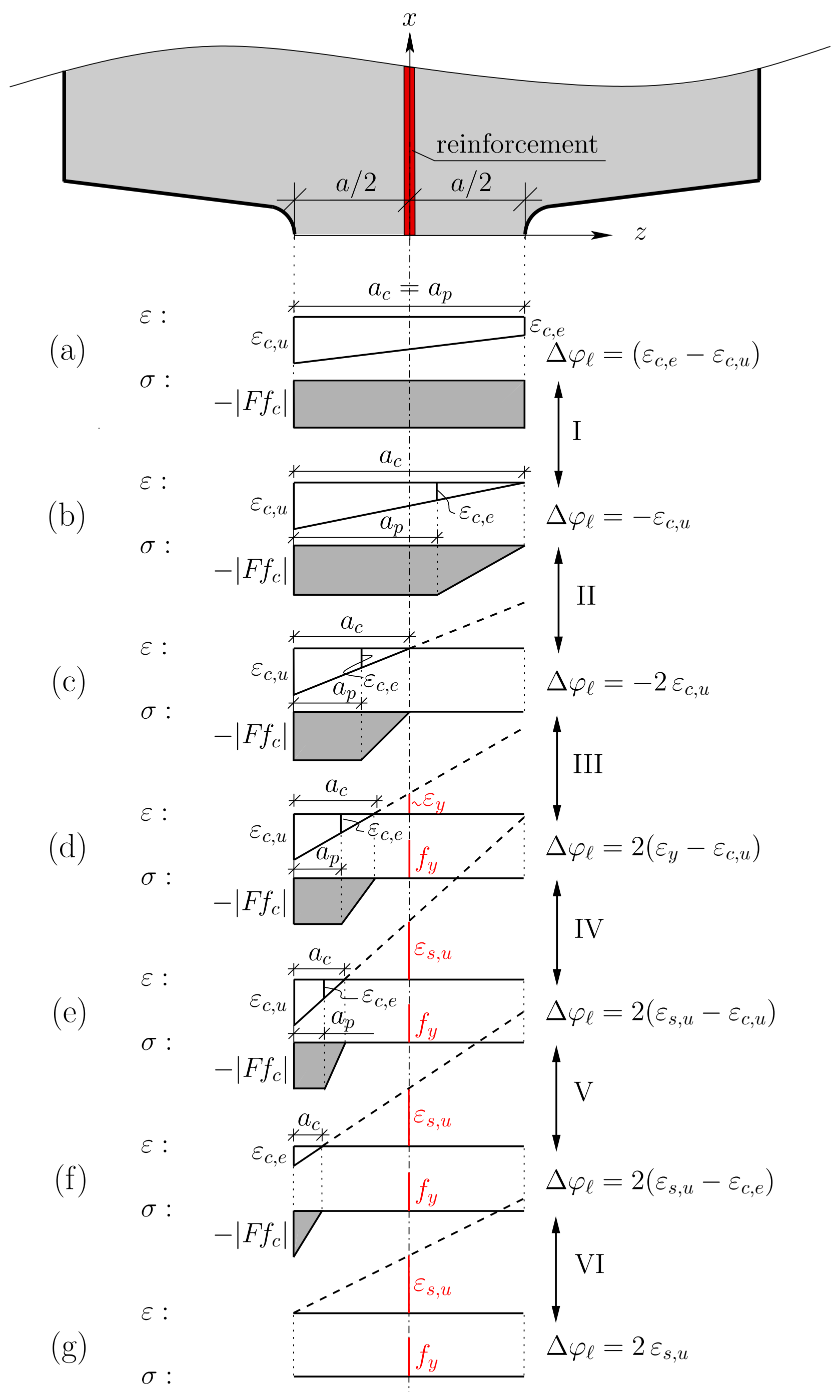


Figure 4: Seven schematic linear strain distributions, referring to ultimate limit states of reinforced concrete hinges, representing boundary scenarios for six operating conditions; and corresponding stress distributions, see also Eqs. (1) and (2)

## 2.3. Ultimate limits of operating condition I

In this case, the ultimate limits are bounded by the scenarios (a) and (b), illustrated in Fig. 4, see also Table 1. The ultimate limit strain of concrete is always reached at the left edge of the neck:

$$\varepsilon_c(z\!=\!-a/2) = \varepsilon_{c,u}\,. \tag{18}$$

At the right edge of the neck, the strain of concrete ranges between $\varepsilon_{c,e}$ and 0, see Fig. 4. The slope of the strain distributions is proportional to the maximum tolerable relative rotation, see Eq. (2). Thus,

$$\text{(a)} \quad \ldots \quad (\varepsilon_{c,e} - \varepsilon_{c,u}) \leq \Delta\varphi_\ell \leq -\varepsilon_{c,u} \quad \ldots \quad \text{(b)}\,, \tag{19}$$

see Fig. 4 and Table 1. The corresponding values of $\Delta\ell_\ell$ follow from inserting Eq. (18) into Eq. (1) and solving the resulting expression for $\Delta\ell_\ell$:

$$\Delta\ell_\ell = a\left(\frac{\Delta\varphi_\ell}{2} + \varepsilon_{c,u}\right). \tag{20}$$

The expression for $a_p$ as a function of $\Delta\ell_\ell$ and $\Delta\varphi_\ell$ is obtained as follows: The value of $z$ at the elastic limit strain is obtained by setting Eq. (1) equal to $\varepsilon_{c,e}$ and solving the resulting expression for $z$. This gives

$$z(\varepsilon\!=\!\varepsilon_{c,e}) = a\frac{\varepsilon_{c,e}}{\Delta\varphi_\ell} - \frac{\Delta\ell_\ell}{\Delta\varphi_\ell}\,. \tag{21}$$

The width of the plastic ligament, $a_p$, is by $a/2$ larger than $z(\varepsilon\!=\!\varepsilon_{c,e})$, see Fig. 4. Thus, $a_p$ follows as

$$a_p = \frac{a}{2} + a\frac{\varepsilon_{c,e}}{\Delta\varphi_\ell} - \frac{\Delta\ell_\ell}{\Delta\varphi_\ell}\,. \tag{22}$$

The degree of utilization, $\nu$, is obtained by inserting $a_c = a$ and $\chi = 0$, see Fig. 4 and Table 1, together with Eq. (22) into Eq. (15), specializing the resulting expression for $\Delta\ell_\ell$ according to Eq. (20), and substituting the obtained expression for $N$ into Eq. (17). This gives

$$\nu = \left[\frac{1}{\Delta\varphi_\ell}\left(\frac{1}{2}\varepsilon_{c,e} - \varepsilon_{c,u}\right) + \frac{1}{2}\frac{\Delta\varphi_\ell}{\varepsilon_{c,e}}\left(\frac{\varepsilon_{c,u}}{\Delta\varphi_\ell} + 1\right)^2\right]. \tag{23}$$

The sought expression for the maximum tolerable relative rotation as a function of $\nu$ follows from solving Eq. (23) for $\Delta\varphi_\ell$ as

$$\Delta\varphi_\ell = \varepsilon_{c,e} \left[ \left( \nu - \frac{\varepsilon_{c,u}}{\varepsilon_{c,e}} \right) - \sqrt{ \left( \nu - \frac{\varepsilon_{c,u}}{\varepsilon_{c,e}} \right)^2 - \left( \frac{\varepsilon_{c,u}}{\varepsilon_{c,e}} - 1 \right)^2 } \right] . \qquad (24)$$

Notably, inserting Eq. (19) into Eq. (23) shows that the operating condition I is related to

$$\nu \in \left[ 1 - \frac{\varepsilon_{c,e}}{2\,\varepsilon_{c,u}} \ ; \ 1 \right] , \qquad (25)$$

see the part of the abscissa between the labels (a) and (b) in Fig. 5.

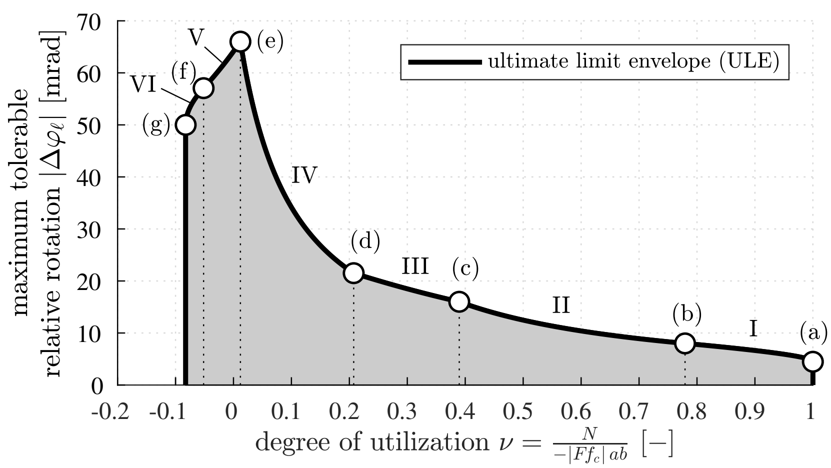


Figure 5: Maximum tolerable relative rotation of reinforced concrete hinges as a function of the degree of utilization of the normal force; evaluation of Eqs. (24), (30), (35), (39), (45), and (49) for $|Ff_c| = 100\,\mathrm{MPa}$, $\varepsilon_{c,e} = -3.53 \times 10^{-3}$, $\varepsilon_{c,u} = -8.00 \times 10^{-3}$, $f_y = 550\,\mathrm{MPa}$, $E_s = 200\,\mathrm{GPa}$, $\varepsilon_y = f_y/E_s$, $\varepsilon_{s,u} = 25.0 \times 10^{-3}$, and $\rho = 1.5\,\%$; $\nu < 0$ refers to the theoretical case of a tensile normal force transmitted across the neck.

### *2.4. Ultimate limits of operating condition II*

In this case, the ultimate limits are bounded by the scenarios (b) and (c), illustrated in Fig. 4, see also Table 1. The ultimate limit strain of concrete is always reached at the left edge of the neck, see Eq. (18). The zero-position of the strain ranges between $z = a/2$ and $z = 0$, see Fig. 4. The slope of the strain distributions is proportional to the maximum tolerable relative rotation, see Eq. (2). Thus,

$$\text{(b)} \quad \ldots \quad -\varepsilon_{c,u} \leq \Delta\varphi_\ell \leq -2\,\varepsilon_{c,u} \quad \ldots \quad \text{(c)}\,, \tag{26}$$

see Fig. 4 and Table 1. The corresponding values of $\Delta\ell_\ell$ are given in Eq. (20).

The expression for $a_c$ as a function of $\Delta\ell_\ell$ and $\Delta\varphi_\ell$ is obtained as follows: The value of $z$ at the zero-position of the strain is obtained by setting Eq. (1) equal to zero and solving the resulting expression for $z$. This gives [5]

$$z(\varepsilon\!=\!0) = -\frac{\Delta\ell_\ell}{\Delta\varphi_\ell}\,. \tag{27}$$

The width of the compressed ligament is by $a/2$ larger than $z(\varepsilon\!=\!0)$, see Fig. 4. Thus, $a_c$ follows as [5]

$$a_c = \frac{a}{2} - \frac{\Delta\ell_\ell}{\Delta\varphi_\ell}\,. \tag{28}$$

The degree of utilization, $\nu$, is obtained by inserting $\chi = 0$ together with Eq. (22) and Eq. (28) into Eq. (15), specializing the resulting expression for $\Delta\ell_\ell$ according to Eq. (20), and substituting the obtained expression for $N$ into Eq. (17). This gives

$$\nu = \frac{1}{\Delta\varphi_\ell}\left(\frac{\varepsilon_{c,e}}{2} - \varepsilon_{c,u}\right). \tag{29}$$

The sought expression for the maximum tolerable relative rotation as a function of $\nu$ follows from solving Eq. (29) for $\Delta\varphi_\ell$ as

$$\Delta\varphi_\ell = \frac{1}{\nu}\left(\frac{\varepsilon_{c,e}}{2} - \varepsilon_{c,u}\right). \tag{30}$$

Notably, inserting Eq. (26) into Eq. (29) shows that the operating condition II is related to

$$\nu \in \left[\,\frac{1}{2}\left(1 - \frac{\varepsilon_{c,e}}{2\,\varepsilon_{c,u}}\right)\;;\;1 - \frac{\varepsilon_{c,e}}{2\,\varepsilon_{c,u}}\,\right], \tag{31}$$

see the part of the abscissa between the labels (b) and (c) in Fig. 5.

### 2.5. Ultimate limits of operating condition III

In this case, the ultimate limits are bounded by the scenarios (c) and (d), illustrated in Fig. 4, see also Table 1. The ultimate limit strain of concrete is always reached at the left edge of the neck, see Eq. (18). The strain of steel at the center of the neck ranges between 0 and $\varepsilon_y$, see Fig. 4. Thus, the maximum tolerable relative rotation ranges in the following interval

$$\text{(c)} \quad \ldots \quad -2\,\varepsilon_{c,u} \leq \Delta\varphi_\ell \leq 2(\varepsilon_y - \varepsilon_{c,u}) \quad \ldots \quad \text{(d)}\,, \tag{32}$$

see Fig. 4, Eq. (2), and Table 1. The corresponding values of $\Delta\ell_\ell$ are given in Eq. (20).

The stress of the steel rebars, $\sigma_s$, is a function of $\Delta\ell_\ell$. It is obtained as follows: The rebars run across the *centerline* of the neck ($y$, $x = z = 0$). Thus, their strain follows from inserting $z = 0$ into Eq. (1) as $\varepsilon_s = \Delta\ell_\ell/a$. Inserting this expression into Eq. (10) delivers

$$\sigma_s = \frac{f_y}{\varepsilon_y}\frac{\Delta\ell_\ell}{a}\,. \tag{33}$$

The degree of utilization, $\nu$, is obtained by inserting $\chi = 1$ together with Eq. (22), Eq. (28), and Eq. (33) into Eq. (15), specializing the resulting expression for $\Delta\ell_\ell$ according to Eq. (20), and substituting the obtained expression for $N$ into Eq. (17). This gives

$$\nu = \frac{1}{\Delta\varphi_\ell}\left(\frac{\varepsilon_{c,e}}{2} - \varepsilon_{c,u}\right) - \left(\frac{\Delta\varphi_\ell}{2} + \varepsilon_{c,u}\right)\frac{f_y}{|Ff_c|}\frac{\rho}{\varepsilon_y}\,. \tag{34}$$

The sought expression for the maximum tolerable relative rotation as a function of $\nu$ follows from solving Eq. (34) for $\Delta\varphi_\ell$ as

$$\begin{aligned}\Delta\varphi_\ell \quad = \quad & \frac{-|Ff_c|}{f_y}\frac{\varepsilon_y}{\rho}\left[\left(\nu + \varepsilon_{c,u}\frac{f_y}{|Ff_c|}\frac{\rho}{\varepsilon_y}\right)\right. \\ & \left. - \sqrt{\left(\nu + \varepsilon_{c,u}\frac{f_y}{|Ff_c|}\frac{\rho}{\varepsilon_y}\right)^2 + 2\frac{f_y}{|Ff_c|}\frac{\rho}{\varepsilon_y}\left(\frac{\varepsilon_{c,e}}{2} - \varepsilon_{c,u}\right)}\,\right].\end{aligned} \tag{35}$$

Notably, inserting Eq. (32) into Eq. (34) shows that the operating condition III is related to

$$\nu \in \left[\,\frac{\frac{1}{2}\varepsilon_{c,e} - \varepsilon_{c,u}}{2(\varepsilon_y - \varepsilon_{c,u})} - \frac{\rho\,f_y}{|Ff_c|}\;;\;\frac{1}{2}\left(1 - \frac{\varepsilon_{c,e}}{2\,\varepsilon_{c,u}}\right)\right], \tag{36}$$

see the part of the abscissa between the labels (c) and (d) in Fig. 5.

### 2.6. Ultimate limits of operating condition IV

In this case, the ultimate limits are bounded by the scenarios (d) and (e), illustrated in Fig. 4, see also Table 1. The ultimate limit strain of concrete is always reached at the left edge of the neck, see Eq. (18). The strain of steel at the center of the neck ranges between $\varepsilon_y$ and $\varepsilon_{s,u}$, see Fig. 4. Thus, the maximum tolerable relative rotation ranges in the following interval

$$\text{(d)} \quad \ldots \quad 2(\varepsilon_y - \varepsilon_{c,u}) \leq \Delta\varphi_\ell \leq 2(\varepsilon_{s,u} - \varepsilon_{c,u}) \quad \ldots \quad \text{(e)}\,, \tag{37}$$

see Fig. 4, Eq. (2), and Table 1. The corresponding values of $\Delta\ell_\ell$ are given in Eq. (20).

The degree of utilization, $\nu$, is obtained by inserting $\chi = 1$ together with Eq. (22), Eq. (28), and $\sigma_s = f_y$ into Eq. (15), specializing the resulting expression for $\Delta\ell_\ell$ according to Eq. (20), and substituting the obtained expression for $N$ into Eq. (17). This gives

$$\nu = \frac{1}{\Delta\varphi_\ell}\left(\frac{\varepsilon_{c,e}}{2} - \varepsilon_{c,u}\right) - \frac{\rho\, f_y}{|Ff_c|}\,. \tag{38}$$

The sought expression for the maximum tolerable relative rotation as a function of $\nu$ follows from solving Eq. (38) for $\Delta\varphi_\ell$ as

$$\Delta\varphi_\ell = \left(\frac{\varepsilon_{c,e}}{2} - \varepsilon_{c,u}\right)\left(\nu + \frac{\rho\, f_y}{|Ff_c|}\right)^{-1}\,. \tag{39}$$

Notably, inserting Eq. (37) into Eq. (38) shows that the operating condition IV is related to

$$\nu \in \left[\,\frac{\frac{1}{2}\varepsilon_{c,e} - \varepsilon_{c,u}}{2(\varepsilon_{s,u} - \varepsilon_{c,u})} - \frac{\rho\, f_y}{|Ff_c|}\;;\;\frac{\frac{1}{2}\varepsilon_{c,e} - \varepsilon_{c,u}}{2(\varepsilon_y - \varepsilon_{c,u})} - \frac{\rho\, f_y}{|Ff_c|}\,\right], \tag{40}$$

see the part of the abscissa between the labels (d) and (e) in Fig. 5.

### 2.7. Ultimate limits of operating condition V

In this case, the ultimate limits are bounded by the scenarios (e) and (f) illustrated in Fig. 4, see also Table 1. The ultimate limit strain of steel is always reached, i.e.

$$\varepsilon(z\!=\!0) = \varepsilon_{s,u}\,. \tag{41}$$

At the left edge of the neck, the strain of concrete ranges between $\varepsilon_{c,u}$ and $\varepsilon_{c,e}$, see Fig. 4. Thus, the maximum tolerable relative rotation ranges in the following interval

$$\text{(e)} \quad \ldots \quad 2(\varepsilon_{s,u} - \varepsilon_{c,u}) \geq \Delta\varphi_\ell \geq 2(\varepsilon_{s,u} - \varepsilon_{c,e}) \quad \ldots \quad \text{(f)}\,, \tag{42}$$

see Fig. 4, Eq. (2), and Table 1. The corresponding value of $\Delta\ell_\ell$ follows from inserting Eq. (41) into Eq. (1) and solving the resulting expression for $\Delta\ell_\ell$ as

$$\Delta\ell_\ell = a\,\varepsilon_{s,u}\,. \tag{43}$$

The degree of utilization, $\nu$, is obtained by inserting $\chi = 1$ together with Eq. (22), Eq. (28), and $\sigma_s = f_y$ into Eq. (15), specializing the resulting expression for $\Delta\ell_\ell$ according to Eq. (43), and substituting the obtained expression for $N$ into Eq. (17). This gives

$$\nu = \left(\frac{1}{2} + \frac{\varepsilon_{c,e}}{2\,\Delta\varphi_\ell} - \frac{\varepsilon_{s,u}}{\Delta\varphi_\ell}\right) - \frac{\rho\, f_y}{|Ff_c|}\,. \tag{44}$$

The sought expression for the maximum tolerable relative rotation as a function of $\nu$ follows from solving Eq. (44) for $\Delta\varphi_\ell$ as

$$\Delta\varphi_\ell = \left(\frac{\varepsilon_{c,e}}{2} - \varepsilon_{s,u}\right)\left(\nu - \frac{1}{2} + \frac{\rho\, f_y}{|Ff_c|}\right)^{-1}\,. \tag{45}$$

Notably, inserting Eq. (42) into Eq. (44) shows that the operating condition V is related to

$$\nu \in \left[\,\frac{-\varepsilon_{c,e}}{4(\varepsilon_{s,u} - \varepsilon_{c,e})} - \frac{\rho\, f_y}{|Ff_c|}\;;\;\frac{\frac{1}{2}\varepsilon_{c,e} - \varepsilon_{c,u}}{2(\varepsilon_{s,u} - \varepsilon_{c,u})} - \frac{\rho\, f_y}{|Ff_c|}\,\right], \tag{46}$$

see the part of the abscissa between the labels (e) and (f) in Fig. 5.

### *2.8. Ultimate limits of operating condition VI*

In this case, the ultimate limits are bounded by the scenarios (f) and (g), illustrated in Fig. 4, see also Table 1. The ultimate limit strain of steel is always reached, see Eq. (41). At the left edge of the neck, the strain of concrete ranges between $\varepsilon_{c,e}$ and 0, see Fig. 4. Thus, the maximum tolerable relative rotation ranges in the following interval

$$\text{(f)} \quad \ldots \quad 2(\varepsilon_{s,u} - \varepsilon_{c,e}) \geq \Delta\varphi_\ell \geq 2\varepsilon_{s,u} \quad \ldots \quad \text{(g)}\,, \tag{47}$$

see Fig. 4, Eq. (2), and Table 1. The corresponding value of $\Delta\ell_\ell$ is given in Eq. (43).

The degree of utilization, $\nu$, is obtained by inserting $\chi = 1$ together with $a_p = 0$, Eq. (28), and $\sigma_s = f_y$ into Eq. (15), specializing the resulting expression for $\Delta\ell_\ell$ according to Eq. (43), and substituting the obtained expression for $N$ into Eq. (17). This gives

$$\nu = \left(\frac{1}{2}\frac{\varepsilon_{s,u}}{\varepsilon_{c,e}} - \frac{1}{2\Delta\varphi_\ell}\frac{\varepsilon_{s,u}^2}{\varepsilon_{c,e}} - \frac{1}{8}\frac{\Delta\varphi_\ell}{\varepsilon_{c,e}}\right) - \frac{\rho\, f_y}{|Ff_c|}\,. \tag{48}$$

The sought expression for the maximum tolerable relative rotation as a function of $\nu$ follows from solving Eq. (48) for $\Delta\varphi_\ell$ as

$$\begin{aligned}\Delta\varphi_\ell \;&=\; 4\,\varepsilon_{c,e}\left[\left(\frac{1}{2}\frac{\varepsilon_{s,u}}{\varepsilon_{c,e}} - \nu - \frac{\rho\, f_y}{|Ff_c|}\right)\right.\\ &\qquad \left. - \sqrt{\left(\frac{1}{2}\frac{\varepsilon_{s,u}}{\varepsilon_{c,e}} - \nu - \frac{\rho\, f_y}{|Ff_c|}\right)^2 - \frac{1}{4}\frac{\varepsilon_{s,u}^2}{\varepsilon_{c,e}^2}}\,\right].\end{aligned} \tag{49}$$

Notably, inserting Eq. (47) into Eq. (48) shows that the operating condition VI is related to

$$\nu \in \left[-\frac{\rho\, f_y}{|Ff_c|}\;;\;\frac{-\varepsilon_{c,e}}{4(\varepsilon_{s,u}-\varepsilon_{c,e})} - \frac{\rho\, f_y}{|Ff_c|}\right], \tag{50}$$

see the part of the abscissa between the labels (f) and (g) in Fig. 5.

*2.9. Design values of elastic and ultimate limit strains of steel and concrete*

The design value of the elastic limit strain of steel, $\varepsilon_{yd}$, is taken from [1, 7]:

$$\varepsilon_{yd} = \frac{f_y}{\gamma_S}\frac{1}{E_{sm}}\,, \tag{51}$$

where $f_y$ denotes the characteristic value of the yield stress, $\gamma_S = 1.15$ stands for the partial safety factor for steel, and $E_{sm}$ denotes its modulus of elasticity. The design value of the ultimate limit strain of steel is obtained as [1, 7]

$$\varepsilon_{s,ud} = 0.9\,\varepsilon_{uk} \approx \frac{\varepsilon_{uk}}{\gamma_S}\,, \tag{52}$$

where $\varepsilon_{uk}$ denotes the characteristic ultimate limit strain of steel according to European design specifications. The Eurocode [1] defines the most unfavorable (= smallest) value of $\varepsilon_{uk}$ as $25 \times 10^{-3}$. This delivers

$$\varepsilon_{s,ud} = 22.5 \times 10^{-3}\,. \tag{53}$$

As for concrete, the design values of the elastic limit strain, $\varepsilon_{c,ed}$, and of the ultimate limit strain, $\varepsilon_{c,ud}$, deserve special considerations. The difference $|\varepsilon_{c,ud} - \varepsilon_{c,ed}|$ defines the length of the stress plateau of concrete in compression in case of ideally-plasticity, see Fig 3 (a). The ductility of concrete decreases with increasing strength, but increases with increasing confinement. Herein, these dependencies are accounted for analogous to regulations of Eurocode 2 [1] and recommendations of the *fib* Model Code 2010 [7].

Regarding unconfined (= *uniaxial*) compression of normal-strength concrete, with strength values in the interval $12\,\mathrm{MPa} \leq |f_{ck}| \leq 50\,\mathrm{MPa}$, the Eurocode 2 [1] and the *fib* Model Code 2010 [7] suggest

$$|\varepsilon^{uni}_{c,ed}| = 1.75 \times 10^{-3} \tag{54}$$

and

$$|\varepsilon^{uni}_{c,ud}| = 3.50 \times 10^{-3}\,. \tag{55}$$

For high-strength concrete, with characteristic strength values larger than 50 MPa, $\varepsilon_{c,ed}$ and $\varepsilon_{c,ud}$ depend on the strength class, see [1, 7] and Table 2.

Table 2: Values of the elastic limit strain and the ultimate limit strain of high-strength concretes C70 and C100, respectively [1, 7]

| | high strength concrete C70 | high strength concrete C100 |
|---|---|---|
| $\lvert\varepsilon^{uni}_{c,ed}\rvert$ | $2.00 \times 10^{-3}$ | $2.40 \times 10^{-3}$ |
| $\lvert\varepsilon^{uni}_{c,ud}\rvert$ | $2.70 \times 10^{-3}$ | $2.40 \times 10^{-3}$ |

With increasing confinement of concrete, the absolute values of both $\varepsilon_{c,ed}$ and $\varepsilon_{c,ud}$ increase. Qualitatively, this is suggested by triaxial experiments, see e.g. [12, 13]. However, some quantitative details are yet not fully understood.

Regarding concrete located in the core of columns containing confining reinforcement, the *fib* Model Code 2010 [7] suggests the following formulae for $\varepsilon_{c,ed}$ and $\varepsilon_{c,ud}$. Based on research by Mander et al. [14, 15], they read as

$$|\varepsilon_{c,ed}| = |\varepsilon_{c,ed}^{uni}| \left[ 1 + 17.5 \left( \frac{\sigma_2}{f_{ck}} \right)^{\frac{3}{4}} \right], \tag{56}$$

and

$$|\varepsilon_{c,ud}| = |\varepsilon_{c,ud}^{uni}| + 0.2 \, \frac{\sigma_2}{f_{ck}} \, , \tag{57}$$

respectively, where $\sigma_2 = \sigma_3$ denotes the effective lateral compressive stress at the ultimate limit state. Concerning reinforced concrete columns, the ratio $\sigma_2/f_{ck}$ amounts to $\approx 0.003$.

Corners of reinforced concrete frames are characterized by larger confinement than reinforced concrete columns. Ultimate limit states under seismic loading frequently refer to plastic hinges, developing at the corners of frames. These regions are strongly reinforced in order to enable the transfer of significant bending moments. The resulting confinement of concrete increases its ultimate limit strain to characteristic values that are two to four-times larger than $|\varepsilon_{c,ud}^{uni}|$, see e.g. [16]:

$$2\,|\varepsilon_{c,ud}^{uni}| \leq |\varepsilon_{c,ud}| \leq 4\,|\varepsilon_{c,ud}^{uni}| \, . \tag{58}$$

The corresponding values of $\sigma_2/f_{ck}$ follow from inserting expressions (58) and Eq. (55) into Eq. (57) as

$$0.0175 \leq \frac{\sigma_2}{f_{ck}} \leq 0.0525 \, . \tag{59}$$

In order to quantify the confinement, which is activated in concrete hinges designed according to the recommendations of Leonhardt and Reimann [6], nonlinear Finite Element simulations were carried out [10]. They revealed that the ratio between the three principal compressive stresses amounts to $1.00 : 0.45 : 0.30$.

The discussed confinement levels are separated by orders of magnitude. The one of reinforced concrete columns is the smallest. It is given as $\approx 0.003$. The one at corners of reinforced concrete frames is by one order of magnitude larger, i.e. $\approx 0.03$, and the one of concrete hinges is another order of magnitude larger, i.e. $\approx 0.3$. This underlines that the Eqs. (56) and (57) should not be expected to be reliable, from a quantitative viewpoint, for assessing the confinement of reinforced concrete hinges. In the interest of developing design recommendations that are based on developments of the *fib* Model

Code 2010, these formulae are nonetheless used for sensitivity analyses. The sensitivity of ultimate limit envelopes (ULE), see Fig. 5, with respect to the confinement parameter $\sigma_2/f_{ck}$ is analyzed in the following section. In order to identify a useful value of $\sigma_2/f_{ck}$, different ultimate limit envelopes are assessed by means of experimental data from bearing capacity tests of reinforced concrete hinges.

## 3. Assessment of the theoretical investigation by means of experimental data

The usefulness of the theoretical investigation is assessed by applying the derived formulae to the analysis of bearing capacity tests of reinforced concrete hinges, see Table 3. Two different test protocols were the basis of the experimental program. Eccentric compression tests were carried out by Schlappal et al. [5, 17], see Subsection 3.1. The normal force and the relative rotation were controlled independently by Schlappal et al. [5], see Subsection 3.2, and by Base [18], see Subsection 3.3.

In order to assess the *measured* experimental data, *expected values* of the material properties of steel and concrete are taken into account when computing ultimate limit envelopes. As for steel, this includes the characteristic value of the yield stress, $f_y$, and the expected value of modulus of elasticity, $E_{sm}$, see Table 3. The expected value of the elastic limit strain follows from Eq. (51) as

$$\varepsilon_y = \frac{f_y}{E_{sm}} = \varepsilon_{yd}\, \gamma_S \,. \tag{60}$$

The expected value of the ultimate limit strain follows from Eq. (52) as

$$\varepsilon_{s,u} = \frac{\varepsilon_{s,ud}}{0.9} \approx \varepsilon_{s,ud}\, \gamma_S \,. \tag{61}$$

As for concrete, the expected material properties include the experimentally determined value of the uniaxial compressive strength, $f_c$. The expected values of the elastic and ultimate limit strains of concrete are obtained, analogous to steel, see Eqs. (60) and (61), from multiplying the corresponding design values, see Eq. (56) and Eq. (57), respectively, with the partial safety factor for concrete, $\gamma_C = 1.5$,

$$|\varepsilon_{c,e}| = |\varepsilon_{c,ed}|\, \gamma_C \,, \tag{62}$$

$$|\varepsilon_{c,u}| \approx |\varepsilon_{c,ud}|\, \gamma_C \,. \tag{63}$$

Table 3: Experimental data taken from Schlappal et al. [17, 5], see A1, A2, A3, B1, B2, B3 and from Base [18], see Base 1, Base 2, Base 3, see also Eqs. (53), (60), and (61)

| Type | $a$ [mm] | $b$ [mm] | $c$ [mm] | $d$ [mm] | $F$ [$-$] | $\lvert f_c \rvert$ [MPa] | $f_y$ [MPa] | $E_{sm}$ [GPa] | $\varepsilon_y$ [$10^{-3}$] | $\varepsilon_{s,u}$ [$10^{-3}$] | $\rho$ [%] | Source |
|---|---|---|---|---|---|---|---|---|---|---|---|---|
| A1 | 75 | 300 | 400 | 250 | 2.00 | 46.88 | 550 | 200 | 2.75 | 25 | 1.30 | [17] |
| A2 | 75 | 300 | 400 | 250 | 2.00 | 45.22 | 550 | 200 | 2.75 | 25 | 1.30 | [5] |
| A3 | 75 | 300 | 400 | 250 | 2.00 | 75.42 | 550 | 200 | 2.75 | 25 | 1.30 | [5] |
| B1 | 150 | 520 | 820 | 500 | 2.18 | 60.42 | 550 | 200 | 2.75 | 25 | 0.87 | [5] |
| B2 | 100 | 620 | 820 | 500 | 1.99 | 59.33 | 550 | 200 | 2.75 | 25 | 1.09 | [5] |
| B3 | 100 | 620 | 820 | 500 | 1.99 | 107.83 | 550 | 200 | 2.75 | 25 | 1.09 | [5] |
| Base 1 | 197 | 152 | 152 | 610 | 1.73 | 58.59 | 550* | 200* | 2.75* | 25* | 0.85 | [18] |
| Base 2 | 197 | 305 | 406 | 610 | 2.00 | 58.59 | 550* | 200* | 2.75* | 25* | 0.85 | [18] |
| Base 3 | 197 | 305 | 406 | 610 | 2.00 | 58.59 | 550* | 200* | 2.75* | 25* | 0.42 | [18] |

* estimated values

Sensitivity analyses with respect to the confinement level were carried out. For each one of the analyzed tests, five ultimate limit envelopes were computed by means of the formulae derived in Section 2 for five particular confinement levels, see the second column in Table 4. Corresponding values of $\varepsilon_{c,e}$ and $\varepsilon_{c,u}$ are also listed in Table 4. They were computed according to Eqs. (54)-(57), Table 2, and Eqs. (62) and (63).

- Normal-strength concrete was used to produce the specimens for the test sets A1, A2, B1, B2, Base 1, Base 2, and Base 3. The corresponding values of $|\varepsilon_{c,ed}^{uni}|$ and $|\varepsilon_{c,ud}^{uni}|$ are given in Eqs. (54) and (55).
- High-strength concrete with $|f_c| \approx 75\,\mathrm{MPa}$ was used to produce the specimens for the test set A3. The corresponding values of $|\varepsilon_{c,ed}^{uni}|$ and $|\varepsilon_{c,ud}^{uni}|$, referring to the strength class C70, are shown in Table 2.
- High-strength concrete with $|f_c| \approx 108\,\mathrm{MPa}$ was used to produce the specimens for the test set B3. The corresponding values of $|\varepsilon_{c,ed}^{uni}|$ and $|\varepsilon_{c,ud}^{uni}|$, referring to the strength class C100, are shown in Table 2.

Notably, the obtained values of $\varepsilon_{c,u}$ are still smaller than ultimate limit strains observed in experiments on plain concrete subjected to triaxial compression [12, 13].

Table 4: Expected values of the elastic limit strain, $\varepsilon_{c,e}$, and of the ultimate limit strain, $\varepsilon_{c,u}$, as functions of the confinement level $\sigma_2/f_{ck}$, according to the *fib* Model Code 2010 [7], for normal-strength concrete and high-strength concretes C70 and C100, see also Eqs. (54)-(57), Table 2, and Eqs. (62) and (63)

| | confinement level | normal-strength concrete | | high-strength concrete C70 | | high-strength concrete C100 | |
|---|---|---|---|---|---|---|---|
| ULE | $\sigma_2/f_{ck}$ $[10^{-2}]$ | $\lvert\varepsilon_{c,e}\rvert$ $[10^{-3}]$ | $\lvert\varepsilon_{c,u}\rvert$ $[10^{-3}]$ | $\lvert\varepsilon_{c,e}\rvert$ $[10^{-3}]$ | $\lvert\varepsilon_{c,u}\rvert$ $[10^{-3}]$ | $\lvert\varepsilon_{c,e}\rvert$ $[10^{-3}]$ | $\lvert\varepsilon_{c,u}\rvert$ $[10^{-3}]$ |
| A | 0.00 | 2.63 | 5.25 | 3.00 | 4.05 | 3.60 | 3.60 |
| B | 0.75 | 3.80 | 7.50 | 4.34 | 6.30 | 5.21 | 5.85 |
| C | 1.50 | 4.59 | 9.75 | 5.25 | 8.55 | 6.30 | 8.10 |
| D | 2.25 | 5.30 | 12.0 | 6.05 | 10.8 | 7.26 | 10.4 |
| E | 3.00 | 5.94 | 14.3 | 6.78 | 13.1 | 8.15 | 12.6 |

### 3.1. Eccentric compression tests by Schlappal et al. (2017/2019)

Schlappal et al. [5, 17] subjected three sets of reinforced concrete hinges to monotonously increasing eccentric compression up to their bearing capacity, see data labeled as A1, A2, and A3 in Table 3. Set A1 refers to three nominally identical specimens, produced with normal-strength concrete and aggregates with maximum diameters of 16 mm, see [17]. Set A2 refers to two nominally identical specimens, normal-strength concrete, and maximum aggregate diameters of 8 mm. Set A3 refers to three nominally identical specimens, high-strength concrete, and maximum aggregate diameters of 8 mm, see [5]. The recorded data of sets A1, A2, and A3 are shown in Figs. 6 (a), (c), and (e), respectively.

Ultimate limit envelopes were computed based on the formulae derived in Section 2, see Figs. 6 (b), (d), and (f). Eqs. (24), (30), (35), (39), (45), and (49) were evaluated based on the geometric dimensions of the tested concrete hinges and the properties of the concrete and the rebars used, see Table 3. As for the values of $\varepsilon_{c,e}$ and $\varepsilon_{c,u}$, sensitivity analyses with respect to five different confinement levels were carried out, see Table 4. Graphs, illustrating the test data, are added to the diagrams showing the ultimate limit envelopes. In the present context of eccentric compression tests, $M$ is directly proportional to $N$. Thus, the relation between $\Delta\varphi$ and $M$ is affine to the one between $\Delta\varphi$ and $\nu$, compare Figs. 6 (a), (c), and (e) with Figs. 6 (b), (d), and (f).

The points at which the graphs of the experimental data intersect the graphs of the ultimate limit envelopes, represent candidates for ultimate limit state values consisting of a specific normal force and a specific relative rotation, see the circles in Figs. 6 (b), (d), and (f). The points concerned in the graphs of the experimental data, see Figs. 6 (a), (c), and (e), are candidates for ultimate limit states (ULS) of the tested concrete hinges.

All of the investigated values of the confinement level result in a conservative assessment of the ultimate limit state of the tested reinforced concrete hinges. The model-predicted ULS values "A" refer to loading states beyond which an additional significant increase of both the bending moment and the relative rotation was experimentally possible, see Figs. 6 (a), (c), and (e). Thus, the model-predicted ULS values "A" appear to be overly conservative. The model-predicted ULS values "D" refer to loading states which are close to the maximum bending moment of the tested specimen. On the other hand, the corresponding limits $\Delta\varphi_\ell$ appear to be still conservative, because

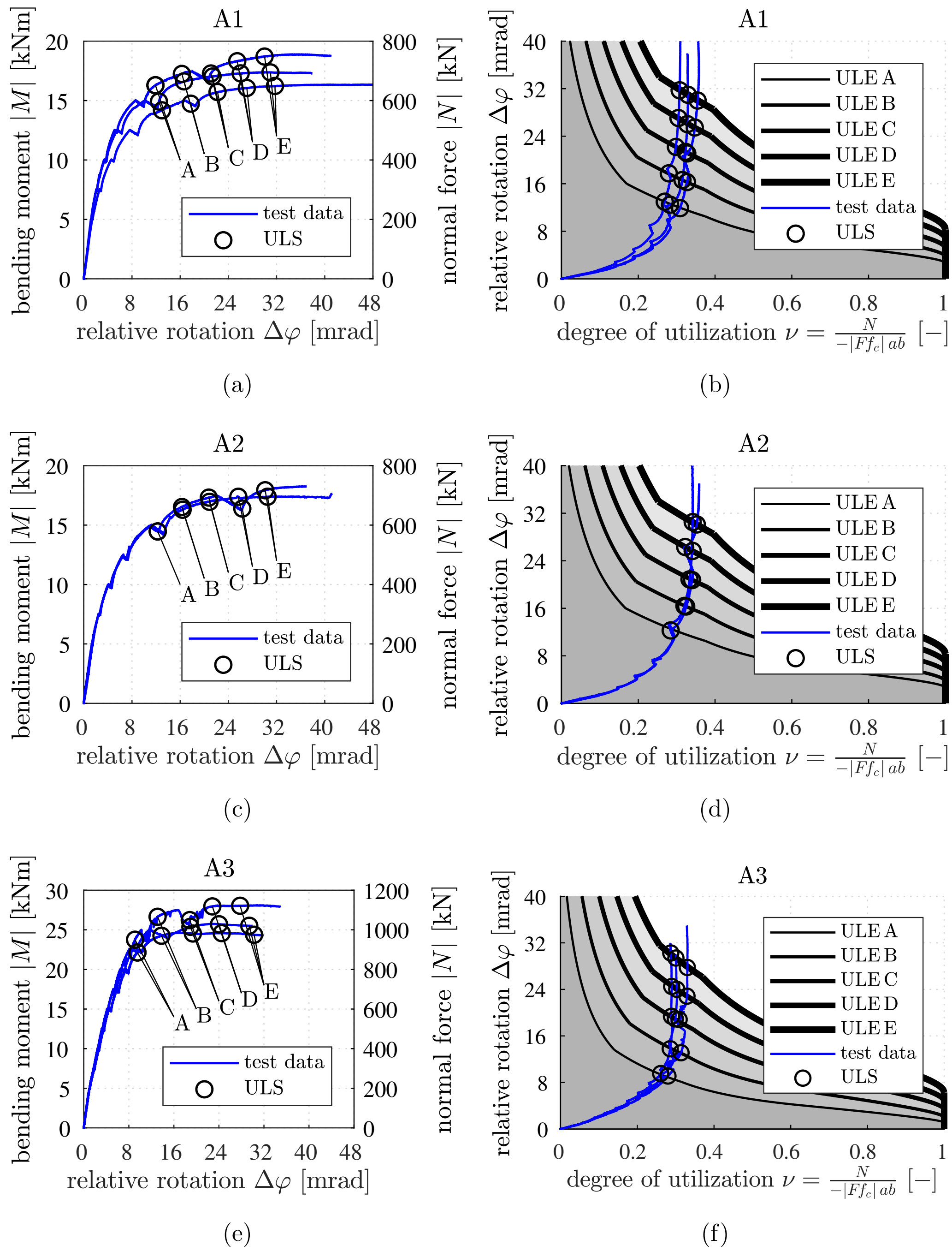


Figure 6: Analysis of eccentric compression tests of reinforced concrete hinges A1, A2, and A3: (a), (c), and (e) show experimental data [5, 17]; (b), (d), and (f) show ultimate limit envelopes computed by means of the formulae derived in Section 2, Table 3, and Table 4

the relative rotation could be increased experimentally to even larger values in all eight analyzed experiments, see Figs. 6 (a), (c), and (e).

### *3.2. Cyclic bending tests by Schlappal et al. (2019)*

Schlappal et al. [5] subjected three types of specimens of reinforced concrete hinges to cyclic bending, see data labeled as B1, B2, and B3 in Table 3. Specimens B1 were produced with an $a/d$-ratio amounting to 0.3, with a normal-strength concrete, specimens B2 with $a/d = 0.2$, with a normal-strength concrete, and specimens B3 with $a/d = 0.2$, with a high-strength concrete. In each one these three cases, three pairs of crossing steel rebars, with a diameter of 1.2 cm, were running across the neck.

Three nominally identical reinforced concrete hinges were produced and tested for each one of the three specimen types, resulting in a total of nine specimens, see Table 3. At first, the specimens were subjected to a specific compressive normal force which was kept constant thereafter. As for the three specimens of type B1, the normal forces amounted to $-1300\,\mathrm{kN}$, $-2600\,\mathrm{kN}$, and $-4500\,\mathrm{kN}$, respectively. The same values of the normal forces were used for the tests on specimens B2. As for specimens B3, these forces amounted to $-2600\,\mathrm{kN}$, $-3500\,\mathrm{kN}$, and $-5400\,\mathrm{kN}$, respectively. Subsequently, relative rotations were imposed in a cyclic fashion and with increasing amplitudes, followed by removal of the applied bending moment. The maximum relative rotation amounted to $\approx 20\,\mathrm{mrad}$. Notably, in the experiments the bearing capacity of the concrete hinges was never reached, see the test results, illustrated in Figs. 7 (a), (b), (c), 8 (a), (b), (c), and 9 (a), (b), (c).

Ultimate limit envelopes were computed based on the formulae derived in Section 2, see Figs. 7 (d), 8 (d), and 9 (d). Eqs. (24), (30), (35), (39), (45), and (49) were evaluated based on the geometric dimensions of the tested concrete hinges and the properties of the concrete and the rebars used, see Table 3. As for the values of $\varepsilon_{c,e}$ and $\varepsilon_{c,u}$, sensitivity analyses with respect to five different confinement levels were carried out, see Table 4. Graphs, illustrating the test data, are added to the diagrams showing the ultimate limit envelopes. In the tests, carried out with a constant normal force, $\Delta\varphi$ was increased and decreased at a constant value of $\nu$, see Figs. 7 (d), 8 (d), and 9 (d). The three experiments each for the three specimen types are highlighted in red, green, and blue, respectively.

The points at which the graphs of the experimental data intersect the graphs of the ultimate limit envelopes, represent candidates for ultimate limit state values consisting of a specific normal force and a specific relative

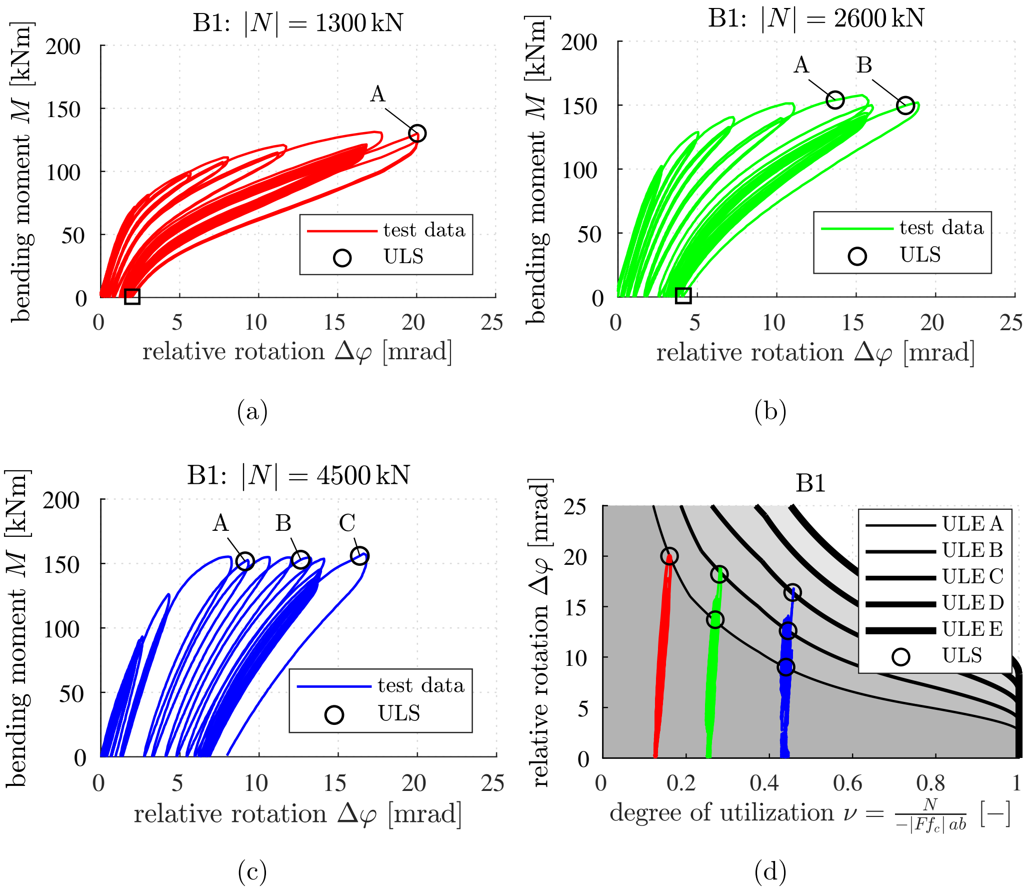


Figure 7: Analysis of tests with cyclic bending, at a constant normal force, on reinforced concrete hinges B1: (a), (b), and (c) show experimental data [5]; (d) refers to identification of ultimate limit envelopes, computed by means of the formulae derived in Section 2, Table 3, and Table 4; the square symbols highlight the residual relative rotations measured at the end of the last test cycles

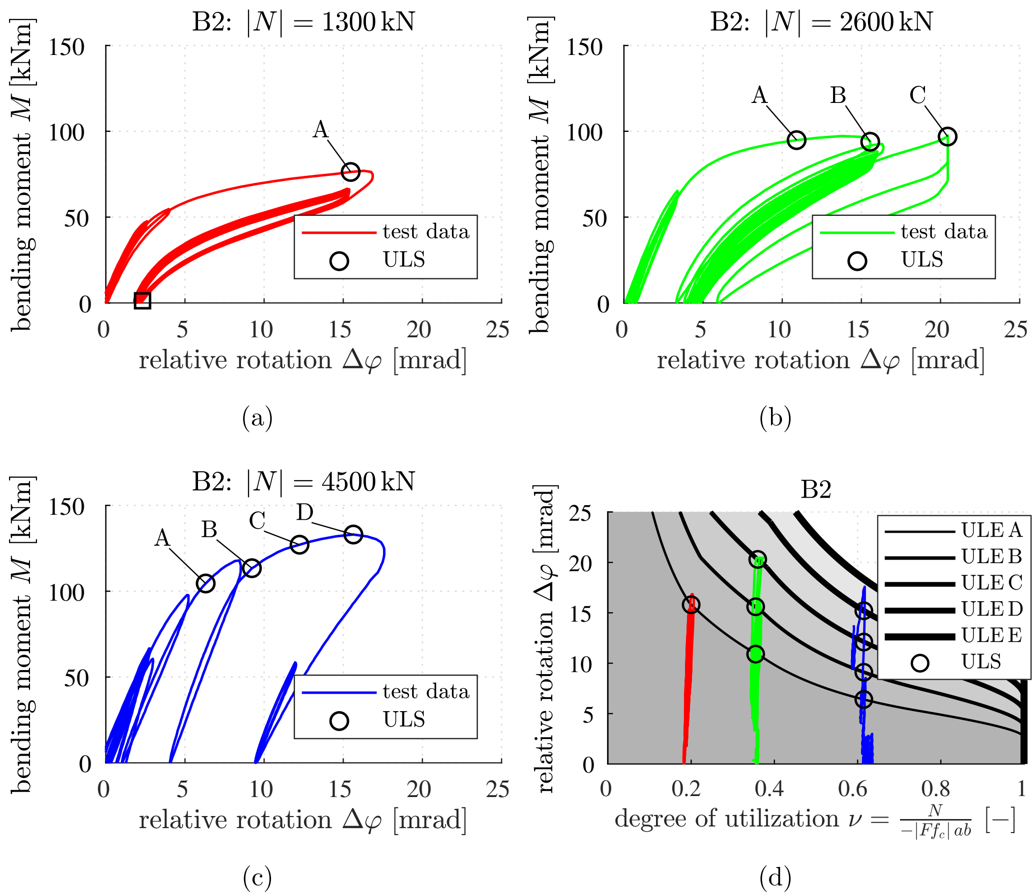


Figure 8: Analysis of tests with cyclic bending, at a constant normal force, on reinforced concrete hinges B2: (a), (b), and (c) show experimental data [5]; (d) refers to identification of ultimate limit envelopes, computed by means of the formulae derived in Section 2, Table 3, and Table 4; the square symbol highlights the residual relative rotation measured at the end of the last test cycle

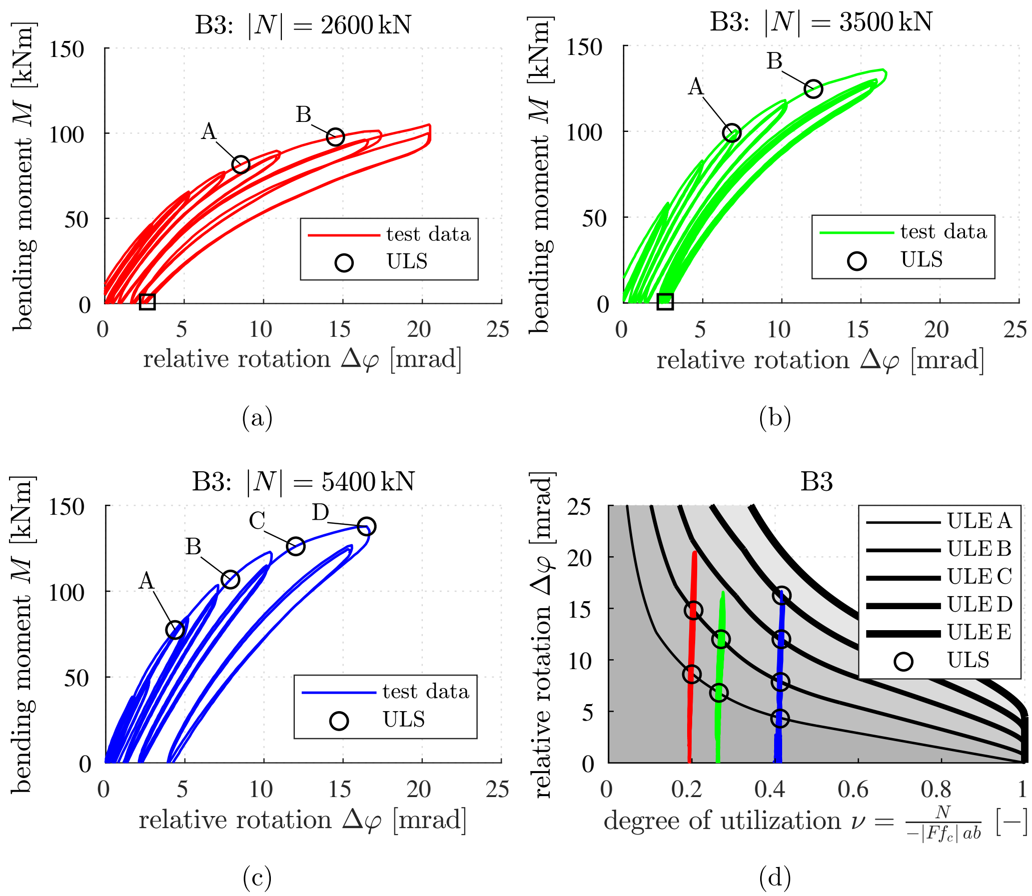


Figure 9: Analysis of tests with cyclic bending, at a constant normal force, on reinforced concrete hinges B3: (a), (b), and (c) show experimental data [5]; (d) refers to identification of ultimate limit envelopes, computed by means of the formulae derived in Section 2, Table 3, and Table 4; the square symbols highlight the residual relative rotations measured at the end of the last test cycles

rotation, see the circles in Figs. 7 (d), 8 (d), and 9 (d). The points concerned in the graphs of the experimental data, see Figs. 7 (a), (b), (c), 8 (a), (b), (c), and 9 (a), (b), (c), are candidates for ultimate limit states (ULS) of the tested concrete hinges.

In four out of the nine tests the model-predicted ULS values "C" were surpassed, see Figs. 7 (c), 8 (b) and (c), as well as 9 (c). As for the other five tests, the small values of residual relative rotations, measured at the end of the last test cycles, i.e. after unloading to $M = 0\,\mathrm{kNm}$, indicate that the respective bearing capacities were far from being reached, see the squares in Figs. 7 (a) and (b), 8 (a), as well as 9 (a) and (b). Thus, ULS values "C" appear to be reasonable.

### *3.3. Experiments by Base (1962)*

Base [18] tested four concrete hinges. Three of them were reinforced. They are labeled as Base 1, Base 2, and Base 3, see Table 3. Their structural performance is described in the following.

The test Base 1, see also the squares in Fig. 10, was carried out as follows: at first, the specimen was subjected to a normal force amounting to $-750\,\mathrm{kN}$. While it was kept constant, the relative rotation was monotonously increased to 25 mrad. Then, it was decreased to 10 mrad. Simultaneously, the absolute value of normal force was increased to $-1480\,\mathrm{kN}$. Finally, the new value of the normal force was kept constant, and the relative rotation was increased up to failure, which occurred at 21 mrad.

The test Base 2, see also the squares in Fig. 11, was carried out as follows: at first, the specimen was subjected to a normal force amounting to $-1450\,\mathrm{kN}$. Then, the relative rotation was increased to 20 mrad, followed by cyclic loading in the interval from 10 mrad to 20 mrad and $-1400\,\mathrm{kN}$ to $-1650\,\mathrm{kN}$, respectively. After 900 cycles, the relative rotation was increased to 70 mrad. Larger values could not be applied by the testing machine. Therefore, the relative rotation was kept constant and the normal force was increased to $-2500\,\mathrm{kN}$. Larger values could not be applied by the testing machine. The specimen did not fail. The test was terminated.

The test Base 3, see also the squares in Fig. 12, was carried out as follows: at first, the specimen was subjected to a normal force amounting to $-760\,\mathrm{kN}$. Then, the relative rotation was increased to 20 mrad, followed by cyclic loading in the interval from 10 mrad to 20 mrad and $-810\,\mathrm{kN}$ to $-990\,\mathrm{kN}$, respectively. After 200 cycles, the relative rotation was increased to 25 mrad. Then, a shear force was imposed and increased to 500 kN. The normal force

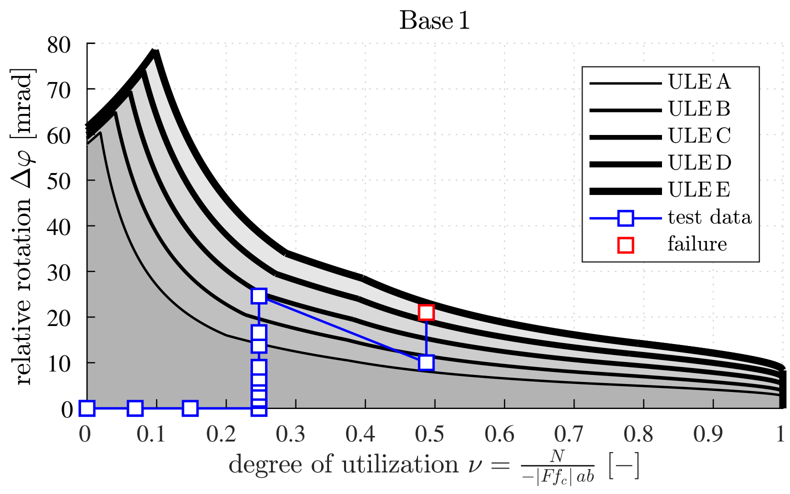


Figure 10: Analysis of the test Base 1: experimental data from [18] and ultimate limit envelopes, computed by means of the formulae derived in Section 2, Table 3, and Table 4

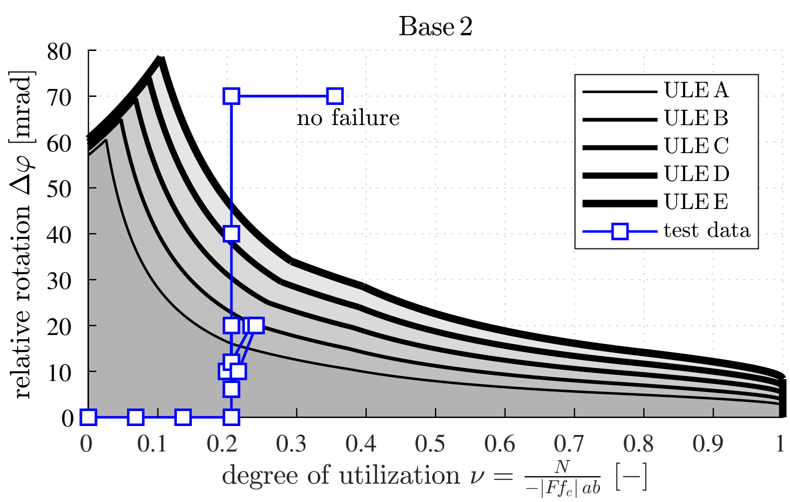


Figure 11: Analysis of the test Base 2: experimental data from [18] and ultimate limit envelopes, computed by means of the formulae derived in Section 2, Table 3, and Table 4

was varied between $-520\,\mathrm{kN}$ and $-820\,\mathrm{kN}$. Finally, the normal force was set equal to $-760\,\mathrm{kN}$, the shear force to $440\,\mathrm{kN}$, and the relative rotation was increased to up failure, which occurred at $64\,\mathrm{mrad}$.

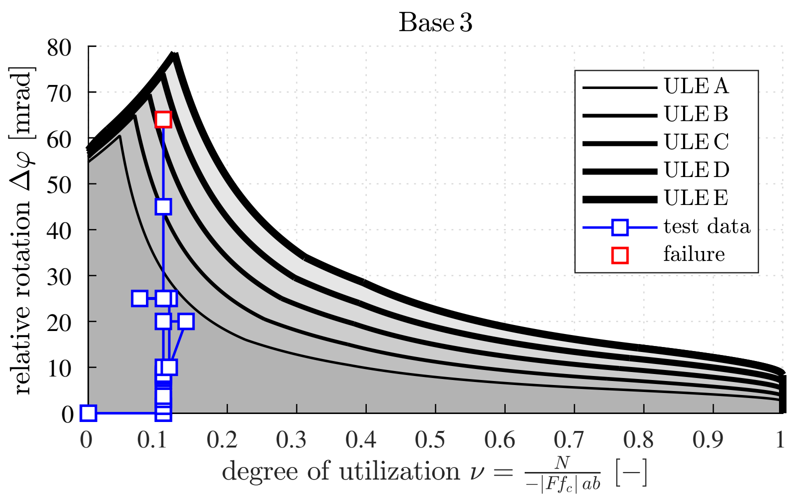


Figure 12: Analysis of the test Base 3: experimental data from [18] and ultimate limit envelopes, computed by means of the formulae derived in Section 2, Table 3, and Table 4

Ultimate limit envelopes were computed for the three tested concrete hinges. The Eqs. (24), (30), (35), (39), (45), and (49) were evaluated based on the geometric dimensions of the concrete hinges and the properties of the concrete and the rebars used, see Table 3. Because Base did not document the quality of the steel used, B550 A was assumed, see Table 3. As for the values of $\varepsilon_{c,e}$ and $\varepsilon_{c,u}$, sensitivity analyses with respect to five specific confinement levels were carried out, see Table 4.

The obtained ultimate limit envelopes are added to the graphs showing the experimental data, see Figs. 10 - 12. The failure states of the specimens Base 1 and Base 3 and the final state of specimen Base 2 are outside the ultimate limit envelope "C", see Figs. 10 - 12. This confirms that ULS values "C" appear to be reasonable.

*3.4. Recommended confinement level for reinforced concrete hinges*

The derived ultimate limit envelopes were assessed by means of experimental data from 20 different tests of reinforced concrete hinges.

- Two specimens failed. The other 18 tests were stopped before failure was observed.

- In 15 tests, *including* the two ones where failure was observed, the ultimate limit envelope "C" was surpassed. In the other five tests, where the specimens *did not fail*, the residual relative rotations were measured after complete unloading. They are rather small. This indicates that the bearing capacities of the reinforced concrete hinges were far from being reached.

It is concluded from the presented analysis of experimental data that the ULS values "C" are reasonably conservative. This refers to a computed confinement value of

$$\frac{\sigma_2}{f_{ck}} = 1.5 \times 10^{-2}\,, \tag{64}$$

see Table 4. Inserting this value into Eqs. (56) and (57) delivers *design* values of the elastic and ultimate limit strains of concrete as

$$|\varepsilon_{c,ed}| = 1.75\,|\varepsilon_{c,ed}^{uni}| \tag{65}$$

and

$$|\varepsilon_{c,ud}| = |\varepsilon_{c,ud}^{uni}| + 3.0 \times 10^{-3}\,. \tag{66}$$

These values are recommended for verification of ultimate limit states of reinforced concrete hinges.

## 4. Verification of ultimate limit states of reinforced concrete hinges in integral bridge construction

The formulae derived in Section 2 were shown to be suitable for description of ultimate limits of reinforced concrete hinges, see Section 3. This was the motivation for using them as the basis for recommendations regarding verification of ultimate limit states in integral bridge construction. Recommendations concerning the layout of the structural dimensions of concrete hinges and verification of serviceability limit states are documented in [5].

### *4.1. Layout of the geometric shape of reinforced concrete hinges*

As for the layout of structural dimensions of concrete hinges, the following recommendations are adopted from Leonhardt and Reimann [6]

$$a \leq 0.3\,d\,, \tag{67}$$

$$t \leq \begin{cases} 0.2\,a\,, \\ 2\,\mathrm{cm}\,, \end{cases} \tag{68}$$

$$\tan\beta \leq 0.1\,, \tag{69}$$

$$b_R \geq \begin{cases} 0.7\,a\,, \\ 5\,\mathrm{cm}\,, \end{cases} \tag{70}$$

see Fig. 1 for the definition of the letter symbols used. Eqs. (67)-(70) ensure that beneficial *triaxial* compressive stress states are activated in the region of the neck and that undesirable tensile macrocracking of concrete is avoided further away from the neck, see [6, 9] and Fig. 13.


(a) (b)

Figure 13: Concrete hinges at the Viaduto de Gonçalo Cristóvão, built in 1961, in Porto, Portugal: (a) shows the structural subsystem; (b) refers to structural damage that could have been avoided, if the conditions (67)-(70) had been respected; after [5].

### *4.2. Verification of ultimate limit states*

It is recommended to use a two-step procedure, referring to the investigation of two bounding scenarios [5].

**Step 1:** The concrete hinge shall be modeled as a classical hinge without bending stiffness, see Fig 14 (a). The structural analysis concerned delivers an *upper* bound of the relative rotation and a *lower* bound of the absolute value of the bending moment: $M = 0\,\mathrm{kNm}$. The design of the concrete hinge is based on computed design values for the normal force $N_d$ and the relative rotation $\Delta\varphi_d$.

**Step 2** The largest bending moment that can be activated at the designed reinforced concrete hinge is calculated. It represents the maximum bending moment that can be carried by the reinforced concrete hinge. The design value of this maximum bending moment, $M_{d,max}$, is imposed on the concrete hinge, and the structural analysis is repeated, see Eq. (74) and Fig 14 (b). This delivers a *lower* bound for the relative rotation and an *upper* bound for the bending moment. The obtained inner forces are the basis for the design of the starter bars and the splitting tensile reinforcement of the adjacent reinforced concrete members. The latter refers to the transport of transverse tensile forces.

Realistic scenarios must fall in between the two analyzed bounds.

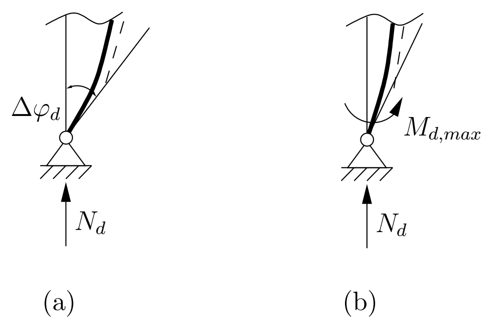


Figure 14: Bounding scenarios for the design of concrete hinges: (a) classical hinge without bending stiffness; (b) application of the design value of the maximum bending moment $M_{d,max}$ to the concrete hinge

As for step 1, quantification of normal forces and relative rotations is based on combinations of permanent loads (index $G$), prestressing (index $P$), and variable loads (index $Q$). The design values of the normal forces, $N_d$, are obtained from the regulations of the Eurocode for structural design of bridges [2, 3, 4]:

$$N_d = \sum_j \gamma_{G,j}\, N_{G,j} + \gamma_P\, N_P + \gamma_{Q,1}\, N_{Q,1} + \sum_{i>1} \gamma_{Q,i}\, \psi_{0,i}\, N_{Q,i}\,, \tag{71}$$

where the coefficients $\psi_{0,i} \leq 1$ account for the small probability that several unfavorable non-permanent actions occur simultaneously. The symbols $\gamma_G$, $\gamma_P$, and $\gamma_Q$ denote the partial safety factors. As for the related design values of the relative rotations, it is recommended to account for visco-elastic stress-relaxation of concrete, which reduces the bending stresses associated with permanent relative rotations [17]. Following Leonhardt and Reimann [6], this can be accounted for by applying a 50 %-reduction to the relative rotations resulting from permanent loads and prestressing, respectively:

$$\Delta\varphi_d = \frac{1}{2}\Big[\sum_j \gamma_{G,j}\,\Delta\varphi_{G,j} + \gamma_P\,\Delta\varphi_P\Big] + \gamma_{Q,1}\,\Delta\varphi_{Q,1} + \sum_{i>1}\gamma_{Q,i}\,\psi_{0,i}\,\Delta\varphi_{Q,i}\,. \quad (72)$$

Given that creep of concrete is simply accounted for by the reduction factor 1/2 in Eq. (72), the value of $E_{cm}$ involved in the elastic part of the analysis refers to the secant modulus of elasticity of concrete [1].

It is recommended to verify the ultimate limit states *after* the serviceability limit states, see [5] and item "A" in Table 5. Thus, the geometric dimensions of the concrete hinge, the reinforcement ratio, the triaxial-to-uniaxial compressive strength ratio, and the strength classes of both concrete and steel are already known. As for the verification of ultimate limit states, the *design* strength values $f_{cd}$ and $f_{yd}$ are relevant, see [1, 7]. The ultimate limit envelope is determined based on Eqs. (24), (30), (35), (39), (45), and (49). As for the values of $\varepsilon_{c,ed}$ and $\varepsilon_{c,ud}$, it is recommended to set the confinement level $\sigma_2/f_{ck}$ equal to $1.50\times10^{-2}$, see also Eqs. (64)-(66). All possible combinations of values of $\nu_d$ and $|\Delta\varphi_d|$ are inserted into the diagram containing the ultimate limit envelope. Thereby, the degrees of utilization $\nu_d$ are quantified according to Eq. (17), based on the computed normal forces, see Eq. (71). An acceptable layout is obtained, if all combinations of $\nu_d$ and $|\Delta\varphi_d|$ are within the ultimate limit envelope.

As for step 2, the maximum of the absolute value of the bending moment that can be activated at the designed reinforced concrete hinge is determined. For that purpose, the Eurocode-inspired interaction envelope, developed by Kalliauer et al. [10] is used. The largest bending moment follows as

$$M_{max} = \frac{1}{8}\,|F f_c| a^2 b\,. \quad (73)$$

As for quantification of the *design* value of the maximum bending moment, $f_c$ in Eq. (73) must be set equal to an *upper* quantile of the uniaxial compressive strength, i.e. to $f_{ck} + 16\,\mathrm{MPa}$, see also [5, 19]. In addition, the partial safety factor for concrete $\gamma_C$ must be applied multiplicatively. Thus, the design value of the maximum bending moment is obtained as

$$M_{d,max} = \frac{\gamma_C}{8}\,F\Big(|f_{ck}| + 16\,\mathrm{MPa}\Big)a^2 b\,. \quad (74)$$

Table 5: Step-by-step design procedure for verification of ultimate limit states of reinforced concrete hinges

A. Verify the serviceability limit states according to Schlappal et al. [5]

B. Model the concrete hinge as a classical hinge without bending stiffness; analyze all load cases

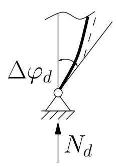


$$N_d = \sum_j \gamma_{G,j}\, N_{G,j} + \gamma_P\, N_P + \gamma_{Q,1}\, N_{Q,1} + \sum_{i>1} \gamma_{Q,i}\, \psi_{0,i}\, N_{Q,i}$$

$$\Delta\varphi_d = \frac{1}{2}\left[\sum_j \gamma_{G,j}\, \Delta\varphi_{G,j} + \gamma_P\, \Delta\varphi_P\right] + \gamma_{Q,1}\, \Delta\varphi_{Q,1} + \sum_{i>1} \gamma_{Q,i}\, \psi_{0,i}\, \Delta\varphi_{Q,i}$$

C. Quantify the degrees of utilization

$$\nu_d = \frac{N_d}{-|Ff_{cd}|\, ab}$$

D. Determine the ultimate limit envelope

1. $$\Delta\varphi_{\ell d} = \varepsilon_{c,ed}\left[\left(\nu_d - \frac{\varepsilon_{c,ud}}{\varepsilon_{c,ed}}\right) - \sqrt{\left(\nu_d - \frac{\varepsilon_{c,ud}}{\varepsilon_{c,ed}}\right)^2 - \left(\frac{\varepsilon_{c,ud}}{\varepsilon_{c,ed}} - 1\right)^2}\,\right] \qquad \nu_d \in \left[1 - \frac{\varepsilon_{c,ed}}{2\,\varepsilon_{c,ud}}\ ;\ 1\right]$$

2. $$\Delta\varphi_{\ell d} = \frac{1}{\nu_d}\left(\frac{\varepsilon_{c,ed}}{2} - \varepsilon_{c,ud}\right) \qquad \nu_d \in \left[\frac{1}{2}\left(1 - \frac{\varepsilon_{c,ed}}{2\,\varepsilon_{c,ud}}\right)\ ;\ 1 - \frac{\varepsilon_{c,ed}}{2\,\varepsilon_{c,ud}}\right]$$

3. $$\Delta\varphi_{\ell d} = \frac{-|Ff_{cd}|}{f_{yd}}\frac{\varepsilon_{yd}}{\rho}\left[\left(\nu_d + \varepsilon_{c,ud}\frac{f_{yd}}{|Ff_{cd}|}\frac{\rho}{\varepsilon_{yd}}\right) - \sqrt{\left(\nu_d + \varepsilon_{c,ud}\frac{f_{yd}}{|Ff_{cd}|}\frac{\rho}{\varepsilon_{yd}}\right)^2 + 2\frac{f_{yd}}{|Ff_{cd}|}\frac{\rho}{\varepsilon_{yd}}\left(\frac{\varepsilon_{c,ed}}{2} - \varepsilon_{c,ud}\right)}\,\right]$$

$$\nu_d \in \left[\frac{\frac{1}{2}\varepsilon_{c,ed} - \varepsilon_{c,ud}}{2(\varepsilon_{yd} - \varepsilon_{c,ud})} - \frac{\rho\, f_{yd}}{|Ff_{cd}|}\ ;\ \frac{1}{2}\left(1 - \frac{\varepsilon_{c,ed}}{2\,\varepsilon_{c,ud}}\right)\right]$$

4. $$\Delta\varphi_{\ell d} = \left(\frac{\varepsilon_{c,ed}}{2} - \varepsilon_{c,ud}\right)\left(\nu_d + \frac{\rho\, f_{yd}}{|Ff_{cd}|}\right)^{-1} \qquad \nu_d \in \left[\frac{\frac{1}{2}\varepsilon_{c,ed} - \varepsilon_{c,ud}}{2(\varepsilon_{s,ud} - \varepsilon_{c,ud})} - \frac{\rho\, f_{yd}}{|Ff_{cd}|}\ ;\ \frac{\frac{1}{2}\varepsilon_{c,ed} - \varepsilon_{c,ud}}{2(\varepsilon_{yd} - \varepsilon_{c,ud})} - \frac{\rho\, f_{yd}}{|Ff_{cd}|}\right]$$

5. $$\Delta\varphi_{\ell d} = \left(\frac{\varepsilon_{c,ed}}{2} - \varepsilon_{s,ud}\right)\left(\nu_d - \frac{1}{2} + \frac{\rho\, f_{yd}}{|Ff_{cd}|}\right)^{-1} \qquad \nu_d \in \left[\frac{-\varepsilon_{c,ed}}{4(\varepsilon_{s,ud} - \varepsilon_{c,ed})} - \frac{\rho\, f_{yd}}{|Ff_{cd}|}\ ;\ \frac{\frac{1}{2}\varepsilon_{c,ed} - \varepsilon_{c,ud}}{2(\varepsilon_{s,ud} - \varepsilon_{c,ud})} - \frac{\rho\, f_{yd}}{|Ff_{cd}|}\right]$$

6. $$\Delta\varphi_{\ell d} = 4\,\varepsilon_{c,ed}\left[\left(\frac{1}{2}\frac{\varepsilon_{s,ud}}{\varepsilon_{c,ed}} - \nu_d - \frac{\rho\, f_{yd}}{|Ff_{cd}|}\right) - \sqrt{\left(\frac{1}{2}\frac{\varepsilon_{s,ud}}{\varepsilon_{c,ed}} - \nu_d - \frac{\rho\, f_{yd}}{|Ff_{cd}|}\right)^2 - \frac{1}{4}\frac{\varepsilon_{s,ud}^2}{\varepsilon_{c,ed}^2}}\,\right]$$

$$\nu_d \in \left[-\frac{\rho\, f_{yd}}{|Ff_{cd}|}\ ;\ \frac{-\varepsilon_{c,ed}}{4(\varepsilon_{s,ud} - \varepsilon_{c,ed})} - \frac{\rho\, f_{yd}}{|Ff_{cd}|}\right]$$

E. Check whether all combinations of $\nu_d$ and $|\Delta\varphi_d|$ are within the ultimate limit envelope

F. Apply the design value of the maximum bending moment to the concrete hinge; re-analyze all load cases

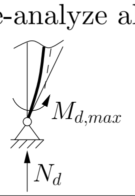


$$M_{d,max} = \frac{\gamma_C}{8} F\Big(|f_{ck}| + 16\,\mathrm{MPa}\Big)\, a^2 b$$

This bending moment is applied to the concrete hinge as the basis for the design of the adjacent parts of the reinforced concrete structure.

### *4.3. Exemplary application to the existing Huyck-bridge*

The Huyck-bridge [8, 20] is a post-tensioned reinforced concrete structure with a span of 43 m, see also [5]. The two abutments are connected to the structure by three reinforced concrete hinges each, see Fig. 15. There are two

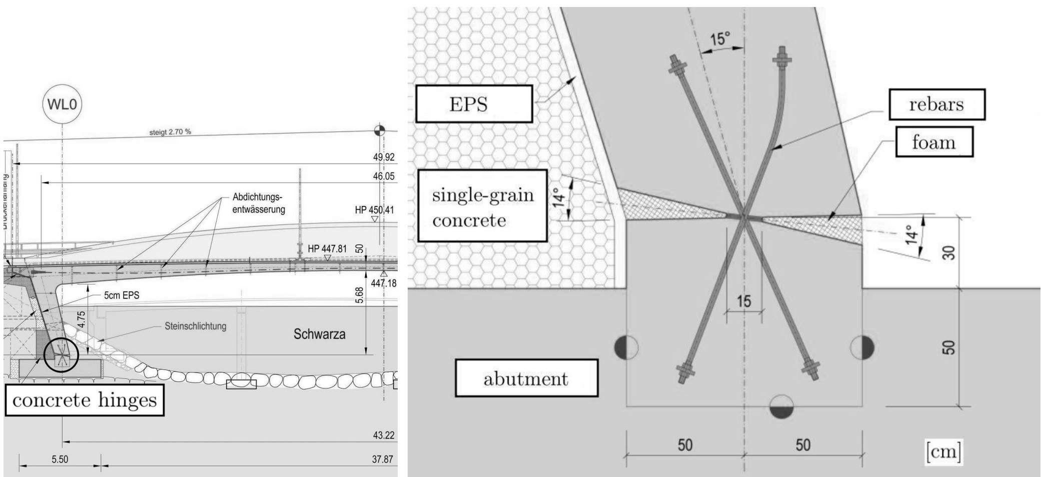


(a) (b)

Figure 15: (a) One half of the longitudinal section, taken from [20], showing the positions of the reinforced concrete hinges, and (b) vertical section through one of the concrete hinges, showing the reinforcement crossing the neck [21]

types of concrete hinges, labeled CH1 and CH2. They differ in the depths of the necks and, thus, in the cross-sectional area, see Table 6.

The reinforced concrete hinges of the Huyck-bridge were designed according to the guidelines of Marx and Schacht [9, 22]. These guidelines are based on the verification of ultimate limit states. They were obtained by translating the design recommendations of Leonhardt and Reimann [6] into the nomenclature of the current Eurocode.

Structural analysis of the Huyck-bridge was carried out according to the regulations of the Eurocode for structural design of bridges [2, 3, 4]. In order to calculate the normal forces and relative rotations, the concrete hinges were modeled as classical hinges without bending stiffness [20, 21]. Design values of the normal forces and the relative rotations were computed according to

Table 6: Material properties of the concrete and the steel rebars and geometric dimensions of the two types of concrete hinges of the Huyck-bridge [21]

| | | |
|---|---|---|
| strength class for concrete: C30 | $\lvert f_{ck} \rvert$ | 30 MPa |
| | $E_{cm}$ | 33 GPa |
| | $\gamma_C$ | 1.50 |
| | $\varepsilon_{c,ed}^{uni}$ | $1.75 \times 10^{-3}$ |
| | $\varepsilon_{c,ud}^{uni}$ | $3.50 \times 10^{-3}$ |
| | $\varepsilon_{c,ed}$ | $3.06 \times 10^{-3}$ |
| | $\varepsilon_{c,ud}$ | $6.50 \times 10^{-3}$ |
| strength class for steel: B550 | $f_{yk}$ | 550 MPa |
| | $E_{sm}$ | 200 GPa |
| | $\gamma_S$ | 1.15 |
| | $\varepsilon_{yd}$ | $2.39 \times 10^{-3}$ |
| | $\varepsilon_{s,ud}$ | $22.50 \times 10^{-3}$ |
| geometric dimensions | $a_1 = a_2$ | 150 mm |
| | $b_1$ | 2250 mm |
| | $b_2$ | 2650 mm |
| | $c_1$ | 3100 mm |
| | $c_2$ | 5275 mm |
| | $d_1 = d_2$ | 1000 mm |
| ratio of triaxial-to-uniaxial compressive strength | $F_1$ | 2.03 |
| | $F_2$ | 2.44 |
| cross-sectional area of the reinforcement | $A_{s1}$ | 12667 $\text{mm}^2$ |
| | $A_{s2}$ | 16286 $\text{mm}^2$ |
| reinforcement ratio | $\rho_1$ | 3.75 % |
| | $\rho_2$ | 4.10 % |

Eqs. (71) and (72). The most unfavorable combinations of the normal forces and the relative rotations are listed in Table 7.

Table 7: Most unfavorable combinations of the relative rotations and the normal forces of the reinforced concrete hinges of the Huyck-bridge, taken from [20, 21]

| | $\lvert\Delta\varphi_d\rvert$ | $\lvert N_d\rvert$ | $\nu_d$ |
|---|---|---|---|
| CH1 | 6.63 mrad | 3402 kN | 0.248 |
| CH2 | 6.63 mrad | 4007 kN | 0.207 |

The design engineers faced a challenge regarding the following condition of the guidelines of Marx and Schacht [9, 22]:

$$ab \leq 12.8 \, \frac{|N_d|}{|\Delta\varphi_d| E_{cm}} \, . \tag{75}$$

Inserting the desired values of $b$ and $E_{cm}$ as well as the calculated values of $|N_d|$ and $|\Delta\varphi_d|$, see Tables 6 and 7, delivered the condition $a < 9\,\text{cm}$. It was concluded that this limitation of the width of the neck does not allow for the proper monolithic production of the structure, because the concrete for the abutments and the lower parts of the concrete hinges must pass through the necks, before being compacted. As a remedy, the consequences resulting from violation of the condition (75) were discussed and assessed very carefully by a team of experienced bridge engineers. Finally, it was agreed to set the width of the necks equal to 15 cm, and to accept the risk that tensile cracking of the concrete hinges may extend beyond half of the width of the neck. This was tolerated because of the stabilizing effect of the reinforcement running across the neck and because of the fact that failure of the concrete hinges does not result in the collapse of the bridge. It was also agreed that further research is needed for a proper scientific justification of the chosen design approach. This resulted in the first research project mentioned in the acknowledgments.

Verification of the ultimate limit states of the reinforced concrete hinges of the Huyck-bridge is re-visited in the context of the approach developed herein. The aforementioned values of $N_d$ are translated into design values of $\nu_d$ according to Eq. (17), see the last two columns of Table 7. The computed pairs of values of $\nu_d$ and $|\Delta\varphi_d|$ are labeled as circles in dimensionless design diagrams, see Fig. 16. Ultimate limit envelopes are added to these diagrams.

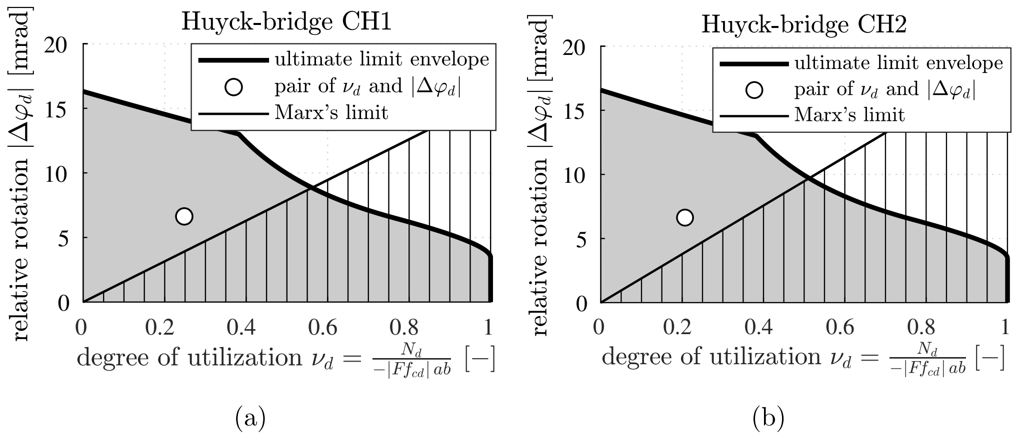


Figure 16: Dimensionless design diagram used for verification of the ultimate limit states of the reinforced concrete hinges of the Huyck-bridge: relative rotations as a function of the degree of utilization of the normal force: concrete hinge (a) CH1 and (b) CH2

They are computed by means of the Eqs. (24), (30), (35), (39), (45), and (49) and of the material and geometric properties of the concrete hinges, see Table 6. The design values of $\nu_d$ and $|\Delta\varphi_d|$ turned out to be *within* the ultimate limit envelopes. Thus, the ultimate limit states are verified *a posteriori*. Finally, it is interesting to add graphs illustrating the violated condition (75) to the dimensionless diagrams of Fig. 16. To this end, the "$\leq$"-sign in condition (75) is replaced by an "="-sign, and the resulting expression is rearranged as

$$\Delta\varphi_d = 12.8\,\frac{|N_d|}{ab\,E_{cm}} = 12.8\,\nu_d\,\frac{|Ff_{cd}|}{E_{cm}}\,, \tag{76}$$

see the by lines shaded areas in Fig. 16. A slight difference between the two types of concrete hinges is observed due to the different ratios of triaxial-to-uniaxial compressive strength, see also Tables 6 and 7.

## 5. Discussion

The present paper is focused on reinforced concrete hinges, transmitting a bending moment and a normal force. According to the investigated ultimate limit states of reinforced concrete hinges, the maximum compressive normal strain of concrete and/or the maximum tensile normal strain of the steel rebars reach the corresponding ultimate limit strain. As regards failure, induced by shear forces and/or yielding of the tensile splitting reinforcement inside the adjacent members, it it is recommended to follow the guidelines of Marx and Schacht [9, 22]. These guidelines are based on experimental observations and theoretical developments of Dix [23], Leonhardt and Reimann [6], as well as Mönnig and Netzel [24].

Noting that there is no experience concerning verification of ultimate limit states with yielding steel rebars, it is recommended to make a conservative estimation of the ductility of steel. According to the Eurocode [1] and Eq. (52), the most unfavorable (= smallest) value of the ultimate limit strain of steel, $\varepsilon_{s,u}$, amounts to $22.5 \times 10^{-3}$. Although this value can be increased up to $67.5 \times 10^{-3}$ when investing into better steel qualities, it is recommended to stay with the smallest value, in order to limit the crack opening displacement inside the neck. Thus, it is recommended to set the ultimate limit strain of steel equal to the most unfavorable value according to European design specifications. Also in the context of the operating conditions IV to VI, in which the steel of the rebars yields, it will be interesting to extend the presented developments to crossed rebars and to account for tension stiffening [25]. However, the typical use of concrete hinges refers to operating conditions I to III, in which the steel of the rebars is behaving in a linear-elastic fashion.

It is worth emphasizing that the Bernoulli-Euler hypothesis was used in order to enable the derivation of easy-to-apply *analytical* formulae as the basis for dimensionless design diagrams. The latter allow practitioners to account, in a simple and customized fashion, for specific geometric and material properties of reinforced concrete hinges. The Bernoulli-Euler hypothesis could be replaced by more enhanced models for reinforced concrete beams, but expectedly at the cost that closed-form solutions turn out of reach.

## 6. Conclusions

The derived analytical formulae and the corresponding dimensionless design diagrams, expressing maximum tolerable relative rotations as a function of the normal force transmitted across reinforced concrete hinges, are useful estimates of ultimate limit states. This was shown by means of relationships between the normal force and the relative rotation, obtained from structural testing of reinforced concrete hinges. 20 tests were carried out, using concrete hinges produced with normal-strength concrete and high-strength concrete. In this context, the following conclusions are drawn:

- Two specimens failed. The other 18 tests were stopped before failure was observed. In 15 tests, *including* the two ones where failure was observed, the recommended ultimate limit envelope was surpassed. In the other five tests, where the specimens *did not fail*, the residual relative rotations were measured after complete unloading. They are rather small. This indicates that the bearing capacities of the reinforced concrete hinges were far from being reached. This underlines that the developed approach is sufficiently conservative for engineering design.

- A trade-off occurs when it comes to the selection of the strength class of concrete. The larger the strength of concrete, the larger are the serviceability limits described in the previous paper [5], but the smaller are the ultimate limits described in the present companion paper. The latter effect is related to the decrease of the ductility of concrete, associated with an increase of the strength of the material.

The present developments can be interpreted as a two-fold extension of the guidelines of Marx and Schacht [9, 22]. The first one refers to the tolerance of bending-induced tensile macrocracking *beyond* one half of the smallest cross-section of the neck. This is acceptable because of the stabilizing role of the reinforcement, which was explicitly accounted for in the underlying mechanical model. The second extension refers to the use of a linear-elastic and ideally-plastic stress-strain relationship for both concrete and steel. Both extensions have turned out to be beneficial to the re-analysis of ultimate limit states of the reinforced concrete hinges of the Huyck-bridge.

The developed design recommendations agree with the following basic principles concerning verification of ultimate limit states according to the *fib* Model Code 2010 [7] and the Eurocode [1, 2, 3, 4]:

- *Linear-elastic and ideally-plastic* material behavior is assumed for concrete in compression and for steel in tension.

- Accepting tensile macrocracking of concrete, the compressive strains of concrete and the tensile strains of steel must stay below the corresponding ultimate limits.

- Elastic limit strains and ultimate limit strains of concrete subjected to triaxial compression were quantified analogous to recommendations of the *fib* Model Code 2010 for reinforced concrete columns.

- The triaxial compressive strength of concrete is estimated based on regulations of Eurocode 2 regarding partially loaded areas.

- Unfavorable choices are made when it comes to quantification of strength values.

- Load combinations are estimated based on the regulations of the Eurocode.

## Acknowledgments

Financial support of the experiments by the Austrian Ministry for Transport, Innovation and Technology (BMVIT), the Austrian Research Promotion Agency (FFG), ÖBB-Infrastruktur AG, and ASFINAG Bau Management GmbH, provided within VIF-project 845681 "Optimierte Bemessungsregeln für dauerhafte bewehrte Betongelenke", is acknowledged. The writers further appreciate discussions with Susanne Gmainer (Smart Minerals GmbH), Alfred Hüngsberg, Andreas Schön, and Hannes Kari (ÖBB-Infrastruktur AG), Erwin Pilch and Michael Kleiser (ASFINAG Bau Management GmbH), as well as the communication of the technical report [21] by Oliver Einhäuser and Alfred Mayerhofer (PCD ZT-GmbH).

Financial support by the Austrian Science Fund (FWF), provided within project P 281 31-N32 "Bridging the Gap by Means of Multiscale Structural Analysis", is also gratefully acknowledged.

## Conflict of interest

The authors declare that they have no conflict of interest.

## References

[1] British Standards Institution, CEN European Committee for Standardization, EN 1992-1-1:2015-07-31 Eurocode 2: Design of concrete structures - Part 1-1: general rules and rules for buildings (2015).

[2] British Standards Institution, CEN European Committee for Standardization, EN 1990:2013-03-15 Eurocode - Basis of structural design (2013).

[3] British Standards Institution, CEN European Committee for Standardization, EN 1990/A1:2013-03-15 Eurocode - Basis of structural design - Amendment 1: Application for bridges (2013).

[4] British Standards Institution, CEN European Committee for Standardization, EN 1991-2:2012-03-01 Eurocode 1: Actions on structures - Part 2: Traffic loads on bridges (2012).

[5] T. Schlappal, J. Kalliauer, M. Vill, S. Gmainer, H. Mang, J. Eberhardsteiner, B. L. Pichler, Serviceability limits of reinforced concrete hinges, Engineering Structures 208 (2020) 109861.

[6] F. Leonhardt, H. Reimann, Betongelenke: Versuchsbericht, Vorschläge zur Bemessung und konstruktiven Ausbildung [Concrete hinges: experiments, design, and execution], Deutscher Ausschuß für Stahlbeton 175 (1965) 1–34, **(in German)**.

[7] CEB-FIP, fib Model Code for Concrete Structures 2010, Ernst & Sohn, Wiley, 2013.

[8] ÖBV-communication, Bautechnik 2016 [Structural engineering 2016], Austrian Society for Construction Technology (2016), **(in German)**.

[9] S. Marx, G. Schacht, Berechnungsmodelle für Betongelenke [Design models for concrete hinges], Prüfingenieur 36 (2010) 15–26, **(in German)**.

[10] J. Kalliauer, T. Schlappal, M. Vill, H. Mang, B. Pichler, Bearing capacity of concrete hinges subjected to eccentric compression: multiscale structural analysis of experiments, Acta Mechanica 229 (2) (2018) 849–866.

[11] J.-L. Zhang, T. Schlappal, Y. Yuan, H. Mang, B. Pichler, The influence of interfacial joints on the structural behavior of segmental tunnel rings subjected to ground pressure, Tunneling and Underground Space Technology 84 (2019) 538–556.

[12] I. Imran, S. Pantazopoulou, Experimental study of plain concrete under triaxial stress, ACI Materials Journal - American Concrete Institute 93 (6) (1996) 589–601.

[13] D. Sfer, I. Carol, R. Gettu, G. Etse, Study of the behavior of concrete under triaxial compression, Journal of Engineering Mechanics 128 (2) (2002) 156–163.

[14] J. B. Mander, M. J. N. Priestley, R. Park, Theoretical stress-strain model for confined concrete, Journal of Structural Engineering 114 (8) (1988) 1804–1826.

[15] J. B. Mander, M. J. N. Priestley, R. Park, Observed stress-strain behavior of confined concrete, Journal of Structural Engineering 114 (8) (1988) 1827–1849.

[16] A. Elghazouli, Seismic design of buildings to Eurocode 8, CRC Press, 2016.

[17] T. Schlappal, M. Schweigler, S. Gmainer, M. Peyerl, B. Pichler, Creep and cracking of concrete hinges – insight from centric and eccentric compression experiments, Materials and Structures 50 (6) (2017) 244.

[18] G. D. Base, Tests on a reinforced concrete hinge with a large design rotation, Cement and Concrete Association, 1962.

[19] B. Tvede-Jensen, M. Faurschou, T. Kasper, A modelling approach for joint rotations of segmental concrete tunnel linings, Tunnelling and Underground Space Technology 67 (2017) 61–67.

[20] PCD ZT-GmbH, Huyckbrücke [Huyck-bridge], Accessed: 2019-11-21, **(in German)**.
URL `https://www.pcd-zt.at/projekte/br%C3%BCcken/huyckbr%C3%BCcke/`

[21] PCD ZT-GmbH: O. Einhäuser, Semmering Basistunnel, Baulos PGG1-Vorhaben Gloggnitz; Straßenbrücke Huyckstraße über die Schwarza; 2010-024, Unpublished technical report (2013), **(in German)**.

[22] S. Marx, G. Schacht, Betongelenke im Brückenbau [Concrete hinges in bridge construction], Berlin Deutscher Beton- und Bautechnik Verein 18 (2010), **(in German)**.

[23] J. Dix, Betongelenke unter oftmals wiederholter Druck- und Biegebeanspruchung [Concrete hinges subjected to frequently repeated axial compression and bending], Deutscher Ausschuß für Stahlbeton 150 (1962) 1–41, **(in German)**.

[24] E. Mönnig, D. Netzel, Zur Bemessung von Betongelenken [Design of concrete hinges], Der Bauingenieur 44 (1969) 433–439, **(in German)**.

[25] J. Kollegger, Tension Stiffening bei schräg zum Riß angeordneten Bewehrungsstäben [Tension stiffening at inclined steel rebars relative to the crack], Bauingenieur 67 (1992) 35–38, **(in German)**.